NASA CR 159635

Department of Aerospace Engineering
and Applied Mechanics
University of Cincinnati

A CALCULATION PROCEDURE FOR VISCOUS FLOW IN TURBOMACHINES - VOL. I

I. KHALIL AND W. TABAKOFF

Supported by:

U.S. Army Research and Technology Laboratories

(AVRADCOM)

Lewis Research Center

Contract No. NAS3-21609

JULY 1979

NASA CR-159635

A CALCULATION PROCEDURE FOR VISCOUS FLOW IN TURBOMACHINES - VOL. I

by

I. Khalil and W. Tabakoff

July 1979

Supported by:

U.S. Army Research and Technology Laboratories

(AVRADCOM)

Lewis Research Center

Contract No. NAS3-21609

1. Report No.	2. Government Accession No.	3. Recipient's Catalog No.
NASA CR 159635		

4. Title and Subtitle	5. Report Date
A CALCULATION PROCEDURE FOR VISCOUS FLOW IN TURBOMACHINES - VOL. I	JULY 1979
	6. Performing Organization Code

7. Author(s)	8. Performing Organization Report No.
I. KHALIL AND W. TABAKOFF	10. Work Unit No.

9. Performing Organization Name and Address	11. Contract or Grant No.
DEPT. OF AEROSPACE ENGINEERING & APPLIED MECHANICS UNIVERSITY OF CINCINNATI CINCINNATI, OHIO 45221	NAS3-21609
	13. Type of Report and Period Covered Contractor Report

12. Sponsoring Agency Name and Address	14. Sponsoring Agency Code
U.S. ARMY RESEARCH & TECHNOLOGY LABORATORIES (AVRADCOM) Propulsion Laboratory Lewis Research Center, Cleveland, Ohio 44135	1L161102AH45

15. Supplementary Notes

Topical report. Project Manager, Dr. Eric R. McFarland, Fluid System Components Division, NASA Lewis Research Center, Cleveland, Ohio 44135.

16. Abstract

A method for analysing the nonadiabatic viscous flow through turbomachine rotors is presented. The field analysis is based upon the numerical integration of the full incompressible stream function-vorticity form of the Navier-Stokes equations, together with the energy equation, over the rotor blade-to-blade stream channels. The numerical code used to solve the governing equations, employs a nonorthogonal boundary-fitted coordinate system that suits the most complicated blade geometries. The effects of turbulence are modelled with the two equations which will be reported in the second volume of this contract. A numerical scheme is used to carry out the necessary integration of the elliptic governing equations.

The method of analysis is applied to various types of turbomachine rotors. First, the flow characteristics within the rotor of a radial inflow turbine are investigated over a wide range of operating conditions. The calculated results are successfully compared to existing experimental data. Second, the flow in a radial compressor is analyzed in order to study the behavior of viscous flow in duffusing cascades. The results are compared qualitatively to known experimental trends. The solution obtained provides a great insight into the flow phenomena that takes place in this type of turbomachines. Comparison with nonviscous flow solutions tend to justify strongly the inadequacy of using these solutions with standard boundary layer techniques to obtain viscous flow details within turbomachine rotors. It is concluded that the method of analysis is quite general and gives a good representation of the actual flow behavior within turbomachine passages.

The computer used in this work is an AMDAHL 470. The flow domain has been divided into 30 step sizes in η direction and 40 in the ξ direction. Typical CPU time was 120 seconds.

17. Key Words (Suggested by Author(s))	18. Distribution Statement
Turbine Aerodynamics Cascade Flow	Unclassified - unlimited STAR Category 02

19. Security Classif. (of this report)	20. Security Classif. (of this page)	21. No. of Pages	22. Price*
UNCLASSIFIED	UNCLASSIFIED	90	

* For sale by the National Technical Information Service, Springfield, Virginia 22161

NASA-C-168 (Rev. 10-75)

TABLE OF CONTENTS

LIST OF FIGURES

LIST OF TABLES

SUMMARY

A method for analyzing the nonadiabatic viscous flow through turbomachine rotors is presented. The field analysis is based upon the numerical integration of the full incompressible stream function-vorticity form of the Navier-Stokes equations, together with the energy equation, over the rotor blade-to-blade stream channels. The numerical code used to solve the governing equations, employs a nonorthogonal boundary-fitted coordinate system that suits the most complicated blade geometries. The effects of turbulence are modelled with the two equations which will be reported in the second volume of this contract. A numerical scheme is used to carry out the necessary integration of the elliptic governing equations.

The method of analysis is applied to various types of turbomachine rotors. First, the flow characteristics within the rotor of a radial inflow turbine are investigated over a wide range of operating conditions. The calculated results are successfully compared to existing experimental data. Second, the flow in a radial compressor is analyzed in order to study the behavior of viscous flow in diffusing cascades. The results are compared qualitatively to known experimental trends. The solution obtained provides a great insight into the flow phenomena that takes place in this type of turbomachines. Comparison with nonviscous flow solutions tend to justify strongly the inadequacy of using these solutions with standard boundary layer techniques to obtain viscous flow details within turbomachine rotors. It is concluded that the method of analysis is quite general and gives a good representation of the actual flow behavior within turbomachine passages.

The computer used in this work is an AMDAHL 470. The flow domain has been divided into 30 step sizes in η direction and 40 in the ζ direction. Typical CPU time was 120 seconds.

INTRODUCTION

For many years it has been recognized that the flow in turbomachines is characterized by the presence of three-dimensional, viscous, and compressible effects occurring in a complex geometrical configuration. The basic understanding of the physical phenomena in this flow requires, therefore, an analysis involving the solution of the unsteady three-dimensional, compressible viscous flow equations within the rotating and stationary blades comprising the machine. Such an analysis is clearly a formidable task. The complexity of the entire problem requires some kind of simplification for one or more of the important factors affecting the flow. These simplifications must cover the essential physical process with sufficient quantitative accuracy and still permit a clear and rational calculation of different flow processes. Most efforts have been concentrated frequently on the solution of the steady and inviscid version of the flow governing equations. These solutions have been marked by increased versatility in the ability to deal with subsonic [1, 2, 3 and 4] as well as transonic flow regimes [5 and 6]. In order to give a more accurate representation of the actual flow processes, approaches [7 and 8] have been devised to account for viscous effects. Most of these approaches are based on the assumption that a two layer model is representative, i.e. an inviscid flow solution which interacts with an end wall boundary layer solution. Important contributions to viscous flow analyses in turbomachinery have been made more recently in References [9, 10 and 11]. The important features of these are the attempts to solve the parabolized version of the complete three-dimensional viscous flow equations with special techniques.

Although the above remarks are not intended to be a complete survey of all the available methods, it is evident that the inviscid analysis is useful for providing a considerable insight into the character of the flow. However, the neglect of viscous effects is a serious shortcoming if detailed quantitative information is desired to calculate viscous losses or heat transfer. The approach

used to account for viscous losses effects by using the boundary layer technique proves to have a number of drawbacks. First, the correct means for matching boundary layer and inviscid solution has not been established if the inviscid flow is rotational, such as in the case of a curved or a rotating passage. Second, most of the existing interacting boundary layer analyses are not capable of handling strong interaction mechanisms of the types present in turbomachine rotors. The parabolic flow approximations, on the other hand, neglect completely the downstream influences. Consequently, important effects such as surface curvature, downstream blockage and reversed flow regions are totally ignored in these type of approximations. To circumvent this deficiency, a procedure based on the solution of the full elliptic Navier Stokes equations is required. Unfortunately, such direct procedures have defied accurate numerical solutions due to the limitations imposed on the core size and speed of present computers. Moreover, the lack of powerful numerical schemes capable of achieving a rapid convergence for three-dimensional elliptic equation renders the solution to be costly.

In the present study, an attempt is made to demonstrate the feasibility of obtaining viscous flow details within turbomachine passages by appropriately combining several blade-to-blade viscous flow solutions. Each of these solutions is obtained through the numerical integration of the full Navier-Stokes equations over a predetermined computational surface that extends between the blades. The set of computational surfaces required for the analysis are themselves generated from the solution of the nonviscous version of the Navier-Stokes equations, as suggested by Wu [1]. Because of the constraints implied by the use of these computational surfaces the resulting viscous flow details are regarded as a quasi-three-dimensional description of the flow field. The use of a non-viscous flow solution tc generate a viscous solution in the manner outlined is anticipated to overcome some of the drawbacks of the method discussed earlier. For example, the inclusion of the full Navier-Stokes equations in the solution procedure makes it possible to account, in an effective manner,

for the interaction between the viscous and inviscid regions. Moreover, preserving the ellipticity of the problem by working with the full equations, besides offering an accurate representation of the flow field, allows for the recognition of downstream influences.

The study will be presented in two parts. The first part which is reported in the present volume deals with the general formulation of the viscous flow equations, and presents the results for laminar flow cases. Turbulent flow cases considered in this investigation will be reported in the second volume.

The present volume consists of four sections described as follows. The equations that govern the flow of viscous fluid within turbomachine passages are presented along with a closure model that accounts for turbulence effects in section 1. A rigorous discussion regarding the accurate representation of the different boundary conditions is also given with special emphasis placed on the determination of the downstream boundary conditions that are required to preserve the ellipticity of the problem. A transformation of the flow equations using a non-orthogonal boundary fitted coordinate system which is numerically generated using Thompson Code [12] is presented in section 2. The overall effect of this transformation is to produce a domain in which the arbitrary blades shapes of the turbomachine become straight and parallel. The details of the numerical scheme used to integrate the flow governing equations as well as the procedures employed to handle the nonlinearities in these equations are given in section 3. Finally, the results of the application of the present method of analysis to various types of turbomachine rotors are presented in section 4.

1. FLOW ANALYSIS

This section presents the detailed development of a method for analyzing the viscous nonadiabatic flow of gas through turbomachine rotors. The partial differential equations that govern the flow behavior within the machine passages are presented first. A transformation of the general equations from the three dimensional form to several particular two dimensional forms, on predetermined stream surfaces, is then outlined. The resulting flow equations are further expressed in the conservation law form using the vorticity-stream function formulation. This is followed by a discussion of the necessary boundary conditions that lead to a unique solution to the problem.

Fundamental Aerothermodynamic Relations

The three dimensional viscous, compressible flow within turbomachine rotors is governed by the following set of laws.

Conservation of Mass:

$$\frac{\partial \rho}{\partial t} + \nabla\cdot(\rho\bar{W}) = 0 \tag{1}$$

Conservation of Momentum:

Newton's second law of motion when combined with Stokes hypothesis can be written as

$$\rho\left(\frac{\partial \bar{W}}{\partial t} + (\bar{W}\cdot\nabla)\bar{W} + 2\bar{\Omega}\times\bar{W} - \frac{\Omega^2}{2}\nabla r^2\right) = -\nabla p - \nabla\times[\mu(\nabla\times\bar{W})] + \frac{4}{3}\nabla(\mu\nabla\cdot\bar{W}) \tag{2}$$

where $\bar{\Omega}$ is the rotor angular velocity.

Conservation of Energy:

In the absence of heat sources or sinks, the first law of thermodynamics for a fluid with a thermal conductivity, K, can be written as:

$$\rho\left(\frac{\partial h}{\partial t} + \bar{W}\cdot\nabla h\right) = \frac{\partial p}{\partial t} + (\bar{W}\cdot\nabla)p + D + \nabla\cdot(K\nabla T) \tag{3}$$

In the previous equations, p, ρ, T, and h denote the static pressure, density, temperature and enthalpy, respectively. While, μ represents the kinematic viscosity coefficient and D is the viscous dissipation function. $\bar{W}$ is the relative velocity vector at any point, whose location is defined by the relative position vector $\bar{r}$, in the rotating frame of reference. The relations among the flow state variables are those of the ideal gas

$$p = \rho RT \tag{4}$$

and $$dh = C_p\, dT \tag{5}$$

The mass-averaged variables principle is utilized in the above equations in order to describe the behavior of a turbulent flow. According to this principle, the components of the velocity vector $\bar{W}$, and the temperature T, are expressed on a mass-averaged basis, while the pressure p and the density ρ are expressed by their mean values only. For any flow variable $Q(x_1,x_2,x_3,t)$, its mass-averaged value, q, is given by:

$$q(x_1,x_2,x_3) = \overline{Q(x_1,x_2,x_3,t)\ \rho^*(x_1,x_2,x_3,t)}/\rho$$

where $\rho^*(x_1,x_2,x_3,t)$ is the instantaneous value of the density at any point whose location is defined by the coordinate (x_1,x_2,x_3). The over bar in the above equation represents the conventional time average, thus $\bar{\rho}^* \equiv \rho$. An effective viscosity μ_e is also used instead of the kinematic viscosity μ. This effective viscosity is assumed to describe the effects of Reynolds stress. In the present work, a two equation turbulence model will be employed to calculate μ_e. The complete details of the model and its implication is outlined in Volume 2 of this study.

Stream Surface Equations

An approach will be taken to reduce the spatial dimensions of the problem from the general three dimensional form to several particular two dimensional forms. The objective is to obtain a

solution to the flow governed by the equations (1) to (5) through an appropriate combination of two dimensional flow solutions. The reduction in spatial dimension is achieved through the consideration of the blade-to-blade stream surface concept. The blade-to-blade stream surface, S_1, may be described by the annulus that would extend from the pressure surface of a blade to the suction surface of the next blade, as shown in Figure 1. This annulus is characterized by the variation of its filament thickness, b, and the radius, r. For the purpose of the present discussion, the stream surface S_1 will be considered to represent the mean geometric properties of the annulus. It is possible to trace out the shapes and the filament thicknesses for a finite number of these blade-to-blade stream surfaces (annuli) in any turbomachine passage, using a meridional flow analysis as that indicated in reference [1]. On these stream surfaces the flow equations (1), (2) and (3) are transformed to several two dimensional mathematical expressions. This is possible since each stream surface provides relations among the coordinates, such that the variation of flow properties over each surface may be described in terms of two space variables only. If a solution to the resulting two dimensional equations is obtained for each stream surface, then the flow properties throughout the three dimensional field may be readily evaluated.

Considering the flow annulus shown in Figure 1. The curvilinear distance along the intersection of the mid-surface of the annulus with a meridional plane is denoted by m. The distance normal to the mid-surface is represented by n. The circumferential coordinate ϕ is considered positive in the counterclockwise direction when viewed down the positive z axis. The thickness of the annulus, b, is assumed to be small compared to the radius r. Hence, the n component of the velocity vector and all variations in the n direction are neglected. The transformation of the flow governing equations (1) and (2) to the stream surface (annulus) coordinate system ($m-\phi-n$) is outlined in Appendix A with the following results.

Continuity:

$$br\frac{\partial \rho}{\partial t} + \frac{\partial}{\partial m}(br\rho W_m) + \frac{\partial}{\partial \phi}(b\rho W_\phi) = 0 \qquad (6)$$

Meridional Momentum:

$$\rho\frac{\partial W_m}{\partial t} + \rho\left(W_m\frac{\partial W_m}{\partial m} + \frac{W_\phi}{r}\frac{\partial W_m}{\partial \phi} - \frac{W^2_\phi}{r}\sin\alpha - \Omega^2 r\sin\alpha - 2\Omega W_\phi\sin\alpha\right)$$

$$= -\frac{\partial p}{\partial m} - \frac{2}{3}\frac{\partial}{\partial m}\left[\mu_e\left(\frac{\partial W_m}{\partial m} + \frac{W_m}{r}\sin\alpha + \frac{1}{r}\frac{\partial W_\phi}{\partial \phi}\right)\right]$$

$$+ \frac{1}{r}\left\{\frac{\partial}{\partial m}\left(2\mu_e r\frac{\partial W_m}{\partial m}\right) + \frac{\partial}{\partial \phi}\left[\mu_e\left(\frac{\partial W_\phi}{\partial m} - \frac{W_\phi}{r}\sin\alpha + \frac{1}{r}\frac{\partial W_m}{\partial \phi}\right)\right]\right.$$

$$\left. - 2\frac{\mu_e}{r}\left[\frac{1}{r}\frac{\partial W_\phi}{\partial \phi} + \frac{W_m}{r}\sin\alpha\right]\sin\alpha\right. \qquad (7)$$

Tangential Momentum:

$$\rho r\frac{\partial W_\phi}{\partial t} + \rho\left(rW_m\frac{\partial W_\phi}{\partial m} + W_\phi\frac{\partial W_\phi}{\partial \phi} + W_m W_\phi\sin\alpha + 2\Omega r W_m\sin\alpha\right)$$

$$= -\frac{\partial p}{\partial \phi} - \frac{2}{3}\frac{\partial}{\partial \phi}\left[\mu_e\left(\frac{\partial W_m}{\partial m} + \frac{W_m}{r}\sin\alpha + \frac{1}{r}\frac{\partial W_\phi}{\partial \phi}\right)\right]$$

$$+ \frac{\partial}{\partial m}\left[\mu_e\left(r\frac{\partial W_\phi}{\partial m} - W_\phi\sin\alpha + \frac{\partial W_m}{\partial \phi}\right)\right] + \frac{\partial}{\partial \phi}\left[2\mu_e\left(\frac{1}{r}\frac{\partial W_\phi}{\partial \phi} + \frac{W_m}{r}\sin\alpha\right)\right]$$

$$+ \mu_e\sin\alpha\left[\frac{\partial W_\phi}{\partial m} - \frac{W_\phi}{r}\sin\alpha + \frac{1}{r}\frac{\partial}{\partial \phi}W_m\right] \qquad (8)$$

where W_m, W_ϕ are the components of the mean relative velocity vector $\bar{W}$ in the meridional and tangential directions, respectively, and α is the angle between the mid-line of the annulus, m, and the axis of rotation, z.

The system of the differential equations (6), (7) and (8), can be written alternatively in terms of a stream function ψ and a vorticity ω. In the present study, the stream function-vorticity formulation is considered for the purpose of reducing the difficulties of the coupling and nonlinearities associated

with the presence of pressure in the flow equations (7) and (8). In addition, this formulation offers the possibility to express the governing equation in their conservative law form. Consequently, no excessive accumulation of errors in the fluxes of the conserved quantities will result in the finite difference approximation of the governing equations. Roache [13] illustrated this by showing how the Gauss divergence theorem is satisfied for the finite difference equations.

For steady state flow, the continuity equation (6) is satisfied by introducing a stream function ψ, which is related to the flow velocity components by:

$$W_m = \frac{\dot{M}}{b} \frac{1}{\rho r} \frac{\partial \psi}{\partial \phi} \qquad \text{and} \qquad W_\phi = - \frac{\dot{M}}{b} \frac{1}{\rho} \frac{\partial \psi}{\partial m} \tag{9}$$

where $\dot{M}$ is the mass flow rate passing through the annulus, S_1, of Figure 1. If the pressure terms are eliminated from equations (7) and (8) by cross differentiation and the mean vorticity variable ω is introduced, one obtains the vorticity transport equation:

$$\frac{\partial}{\partial m} \left(\frac{\dot{M}}{b} \frac{\partial \psi}{\partial \phi} \omega\right) - \frac{\partial}{\partial \phi} \left(\frac{\dot{M}}{b} \frac{\partial \psi}{\partial m} \omega\right) - \frac{\partial}{\partial m} \left[r \frac{\partial}{\partial m} (\mu_e \omega)\right]$$

$$+ \frac{\partial}{\partial \phi} \left[\frac{1}{r} \frac{\partial}{\partial \phi} (\mu_e \omega)\right] + G_1 = 0 \tag{10}$$

where $$W^2 = W_m^2 + W_\phi^2 \tag{11}$$

$$G_1 = 2\Omega \left[\frac{\partial}{\partial m} \left(\frac{\dot{M}}{b} \sin\alpha \frac{\partial \psi}{\partial \phi}\right) - \frac{\partial}{\partial \phi} \left(\frac{\dot{M}}{b} \sin\alpha \frac{\partial \psi}{\partial m}\right)\right]$$

$$+ \frac{\partial \rho}{\partial m} \frac{\partial W^2/2}{\partial \phi} - \frac{\partial \rho}{\partial \phi} \frac{\partial W^2/2}{\partial m} + \Omega^2 r \sin\alpha \frac{\partial \rho}{\partial \phi} \tag{12}$$

and ω is defined by:

$$\omega = \frac{1}{r} \left[\frac{\partial}{\partial m} (r W_\phi) - \frac{\partial}{\partial \phi} (W_m)\right] \tag{13}$$

When the velocities W_m and W_ϕ in equation (13) are expressed in terms of the stream function variable, as defined in equation (9), equation (13) would reduce to the stream function equation:

$$\omega = -\frac{1}{r}\left[\frac{\partial}{\partial m}\left(\frac{\dot{M}r}{b\rho}\frac{\partial\psi}{\partial m}\right) + \frac{\partial}{\partial\phi}\left(\frac{\dot{M}}{b\rho r}\frac{\partial\psi}{\partial\phi}\right)\right] \tag{14}$$

Energy Equation

For a turbomachine rotor it is convenient to express the energy equation in terms of the total enthalpy (H) of the gas, besides its velocity components. The total enthalpy for turbulent flow is expressed as follows:

$$H = C_p T + \frac{W^2}{2} + \Omega W_\phi r + \frac{\Omega^2 r^2}{2} + E \tag{15}$$

where E is the kinetic energy of turbulence. Thus, the energy equation (3), when transformed to the stream annulus coordinate system, as given in Appendix A, can be written as:

$$\begin{aligned}
&\frac{\dot{M}}{b}\left[\frac{\partial}{\partial m}\left(H\frac{\partial\psi}{\partial\phi}\right) - \frac{\partial}{\partial\phi}\left(H\frac{\partial\psi}{\partial m}\right)\right] - \frac{\partial}{\partial m}\left(\frac{\mu_e}{Pr}\, r\frac{\partial H}{\partial m}\right) - \frac{1}{r}\frac{\partial}{\partial\phi}\left(\frac{\mu_e}{Pr}\frac{\partial H}{\partial\phi}\right) \\
&+ \frac{\partial}{\partial m}\left\{\mu_e r\left[\frac{1}{Pr}\frac{\partial W^2/2}{\partial m} - \left(\frac{1}{S_{CE}} - \frac{1}{Pr}\right)\frac{\partial E}{\partial m}\right]\right\} \\
&+ \frac{\partial}{\partial\phi}\left\{\frac{\mu_e}{r}\left[\frac{1}{Pr}\frac{\partial W^2/2}{\partial\phi} - \left(\frac{1}{S_{CE}} - \frac{1}{Pr}\right)\frac{\partial E}{\partial\phi}\right]\right\} - W_\phi\frac{\partial}{\partial m}\left(\mu_e\omega\right) \\
&+ \frac{W_m}{r}\frac{\partial}{\partial\phi}\left(\mu_e\omega\right) - Dr + G_2 = 0
\end{aligned} \tag{16}$$

where Pr is the turbulent Prandtl number and S_{CE} is the turbulent Schmidt number for the kinetic energy of turbulence, E. The source term G_2 in the above equation represents the generation or decay in energy, due to the effect of rotation. It is given by:

$$G_2 = -\Omega \frac{\dot{M}}{b} \{\frac{\partial}{\partial m}[(W_\phi r + r^2\Omega) \frac{\partial \psi}{\partial \phi}] - \frac{\partial}{\partial \phi}[(W_\phi r + r^2\Omega) \frac{\partial \psi}{\partial m}]\}$$

$$+ \Omega\{\frac{\partial}{\partial m}[\frac{\mu_e}{Pr} r \frac{\partial}{\partial m}(W_\phi r + \frac{\Omega r^2}{2})] + \frac{1}{r}\frac{\partial}{\partial \phi}[\frac{\mu_e}{Pr}\frac{\partial}{\partial \phi}(W_\phi r + \frac{\Omega r^2}{2})]\} \quad (17a)$$

The dissipation function, D, can be written as

$$D = 2\mu_e \{(\frac{\partial W_m}{\partial m})^2 + (\frac{1}{r}\frac{\partial W_\phi}{\partial \phi} + \frac{W_m}{r}\sin\alpha)^2\}$$

$$+ \mu_e \{\frac{\partial W_\phi}{\partial m} + \frac{1}{r}\frac{\partial W_m}{\partial \phi} - \frac{W_\phi}{r}\sin\alpha\}^2 \quad (17b)$$

The properties of flow passing through the stream annulus S_1, are completely defined by equations (4), (9), (10), (14) and (16) together with the known variations of μ_e, Pr and the given boundary conditions. The effective viscosity, μ_e, is calculated from a two equation model, one expressing the development of the turbulent kinetic energy, E, and the other its dissipation rate, ε. These equations may be expressed in terms of the stream annulus system of coordinates (m,ϕ,n) as follows:

Turbulent Kinetic Energy Equation:

$$\frac{\dot{M}}{b}[\frac{\partial}{\partial m}(E\frac{\partial \psi}{\partial \phi}) - \frac{\partial}{\partial \phi}(E\frac{\partial \psi}{\partial m})] - \frac{\partial}{\partial m}(\frac{\mu_e}{S_{CE}} r \frac{\partial E}{\partial m})$$

$$+ \frac{\partial}{\partial \phi}(\frac{\mu_e}{S_{CE}}\frac{\partial E}{r\partial \phi}) - rD + \rho\varepsilon r = 0 \quad (18)$$

Dissipation Rate Equation:

$$\frac{\dot{M}}{b}[\frac{\partial}{\partial m}(\varepsilon\frac{\partial \psi}{\partial \phi}) - \frac{\partial}{\partial \phi}(\varepsilon\frac{\partial \psi}{\partial m})] - \frac{\partial}{\partial m}(\frac{\mu_e}{S_{C\varepsilon}} r \frac{\partial \varepsilon}{\partial m})$$

$$+ \frac{\partial}{\partial \phi}(\frac{\mu_e}{S_{C\varepsilon}}\frac{1}{r}\frac{\partial \varepsilon}{\partial \phi}) - \bar{C}_1\frac{\varepsilon}{E} rD + \bar{C}_2\frac{\varepsilon^2}{E}\rho r = 0 \quad (19)$$

where $S_{C\varepsilon}$ is the turbulent Schmidt number for the dissipation of kinetic energy of turbulence, ε. The values of the constants $\bar{C}_1$, $\bar{C}_2$, C_D, S_{CE} and $S_{C\varepsilon}$ in the turbulence model are given in Table 1.

TABLE 1. VALUES OF THE EMPIRICAL CONSTANTS FOR THE k-ε MODEL OF TURBULENCE

C_D	$\bar{C}_1$	$\bar{C}_2$	S_{CE}	$S_{C\varepsilon}$
0.09	1.42	1.92	1.0	1.3

The expession for the effective viscosity μ_e is given by

$$\mu_e = \mu_\ell + C_D \frac{\rho E^2}{\varepsilon} \tag{20}$$

where the laminar viscosity, μ_ℓ, is considered in the present study to be uniform and known.

In general, equations (4) through (20) are valid for any turbomachine geometry or any number of stream annuli except for the two stream annuli $S1_O$ and $S1_N$ shown in Figure 2, which contain the hub and shroud contours. This exception may be attributed to the existence of a large variation in flow properties along the normal, $\bar{n}$, to these two annuli resulting from the presence of the solid boundaries. The determination of the flow properties within these stream annuli constitute a study by itself and is not intended for inclusion in the present work.

The solution of the above system of equations within the turbomachine passages is carried out numerically. One can observe that equations (10), (14), (16), (18) and (19), constitute a system of coupled elliptic partial differential equations, involving second order derivatives of ψ, ω, H, E, and ε which are the dependent variables. From the nature of the problem, none of the terms are negligible in the governing equations. The convective terms

introduce nonlinearity and also instability if the proper differences are not taken into account. Once a solution for these variables has been obtained, the velocity distribution can be determined from equation (9). The pressure distribution can then be evaluated from either equations (7) or (8).

Description of the Computational Domain in the Physical Space

In order to solve the elliptic equations by the usual numerical methods, it is necessary to define a region in the physical domain with boundary conditions specified for the different dependent variables on all boundaries. The flow region of interest, as shown in Figure 3, contains the blade row and segments of the stream surface, S_1, extending upstream and downstream of the row. Due to the circumferential periodicity in the turbomachine passages, the selected domain need to encompass only a fraction of the flow annulus containing a single blade to blade passage. The shape and location of the periodic boundaries (AB, NM, IH and FG) may be defined arbitrarily as long as their spacing corresponds to the blade pitch. The upstream and downstream boundaries (AN, GH) are located sufficiently far from the blade so that the tangential variation in flow properties along them is negligible. The flow properties are consequently considered to be uniform along the boundary AN and GH.

Boundary Conditions

In specifying the boundary conditions, two flow cases are investigated. Preliminarily, only the case of the laminar flow is considered in this report. The turbulent flow case will be reported in a second report. Accordingly, in the following specification of boundary conditions, no assignment for the boundary values of E and ε in equations (18) and (19) is needed. Moreover, the flow properties within the turbomachine channels will be completely defined through the simultaneous solution of equations (10), (14) and (16).

a. The Upstream Boundary AN:

It is a common practice in turbomachine flow calculations that the magnitude and direction of the flow velocities, the total temperature, and the total pressure or density are defined at the turbomachine inlet. Therefore, along the boundary AN, the values of ψ, ω, H or their derivatives can be evaluated using the defined flow properties. The known magnitude of the inlet relative velocity and its direction, as shown in Figure 3, specify the values of $\partial\psi/\partial m$ and $\partial\psi/\partial\phi$ according to the following relations:

$$\frac{\partial\psi}{\partial m} = -\frac{b\rho}{\dot{M}} W_\phi = -\frac{1}{r}\frac{\partial\psi}{\partial\phi}\tan\beta_{inlet}$$

$$\frac{\partial\psi}{\partial\phi} = \frac{b\rho r}{\dot{M}} W_m = \frac{1}{2\pi/Z} \qquad (21)$$

where Z is the number of blades. Since the inlet stream of gas is considered to be uniform, the absolute value of the vorticity ω has to be zero along the boundary AN. In a rotating frame of reference, the relative value of ω is given by the following expression:

$$\omega = -[2\Omega \sin\alpha]_{inlet} \qquad (22)$$

The value for the total enthalpy, H, can be defined using the specified flow properties.

b. The Periodic Boundaries AB, NM and FG, IH:

The periodicity condition requires that the direction and magnitude of the flow velocity as well as other fluid properties be equal at every two corresponding points along AB and MN. Similarly, the same conditions should apply at every two corresponding points along FG and IH. In terms of the present dependent variables, the periodicity requirements are satisfied through the following conditions. First by equating ω, $\partial\omega/\partial\phi$,

$\partial\psi/\partial\phi$, H and $\partial H/\partial\phi$; values at each two corresponding points. Second, ensuring that the ψ values differ by unity between the corresponding points.

c. The Blades Surfaces Boundaries MI and BF:

For the laminar flow case, two boundary conditions over the blade surfaces are usually specified. These are the non-slip condition and the impermeability of the surface in the case of blades with no injection. The non-slip condition requires that

$$\frac{\partial\psi}{\partial N} = 0 \tag{23}$$

where N is the normal to the blade surface. On the other hand the impermeability condition requires the component of velocity in the direction normal to the blade surface to vanish. Therefore, the blade surfaces are treated as streamlines with the ψ values specified as zero on the MI surface and unity on the BF surface. On either MI or BF surfaces, one has therefore, two boundary conditions for ψ but none for ω. It is a well accepted fact in computational fluid mechanics to rely on a modified evaluation of equation (14) to determine the boundary condition for ω. The modification is introduced in an attempt to insure that equation (23) holds, that is, to satisfy the no slip condition. This approach is utilized in the current study to determine the value of the vorticity, ω, over the blade surfaces. The details of the procedures used will be presented in the next section.

In regard to the thermal boundary conditions either the blade surface temperature is known or the normal derivative $\partial T/\partial\eta$ is specified as zero for the adiabatic wall conditions. In either case, equation (15) is used to determine the value of H or its derivative along the blades surfaces.

d. The Downstream Boundary GH:

A few basic problems arise in the specification of the boundary functions for the dependent variables along GH. The

first concerns the bheavior of the dependent variables H and ω. The nature of the problem is that, physically, these are known only if the boundary GH is located at an arbitrarily large distance from the blade surface. In this case the value of H and ω is that of the corresponding surroundings. The placement of GH at exceedingly large distances from the blade boundary is quite obviously not possible for numerical considerations. Therefore, one has to employ some auxiliary conditions, usually obtained by experience, to define H and ω implicitly. The conditions of zero gradients in the meridional direction, m, is employed in the current work.

$$\frac{\partial H}{\partial m} = 0 \tag{24a}$$

For the vorticity, ω, the absolute value is taken to be zero, hence,

$$\omega = - [2\Omega \sin\alpha]_{exit} \tag{24b}$$

More important than the specification of the remote boundary functions of ω and H along GH is the determination of the ψ values at the same boundary. The downstream flow velocities, which may be used to determine the stream function derivatives along GH, and that guarantee a unique solution to the problem are not known in general apriori. Therefore, one has to introduce a supplementary condition, generally resulting from physical intuition, to define the stream function derivatives. Investigators working in the inviscid flow area dealt with this problem by using an iteration procedure, through which the Kutta condition for tangency of the flow at the blade trailing edge is satisfied. This is equivalent to specifying a unique solution to the problem. Unfortunately, the Kutta condition cannot be applied realistically to solve the present flow problem due to the viscosity effects. The conservation of angular momentum principle [14] is employed as an alternative supplementary condition that results

in the required unique solution. The iterative procedure used to implement this condition is as follows.

Estimated exit flow angles, β_{exit}, along GH are used to specify the values of stream function derivatives in the m direction through the following relation:

$$\frac{\partial \psi}{\partial m} = \frac{1}{2\pi/Z} \frac{\tan\beta_{exit}}{r_{exit}} \tag{25}$$

The flow field equations are then solved for the boundary function of ψ given by equation (25) to obtain the velocity and the pressure distribution throughout the stream annulus S_1 of Fig. 1. An evaluation of the torque developed by the annulus is obtained through the integration of the pressure and shear forces acting on the blade surfaces. The change in the angular momentum between the known inlet and the estimated exit flow conditions is determined. If the value of the predicted torque was not equal to the rate of change of the angular momentum, then the direction of the exit flow velocity is altered. The whole procedure is repeated until a satisfactory result is obtained.

The solution of equations (10), (14) and (16), subjected to the above boundary conditions within the blade rows and in the near field, are carried out numerically. In this connection, it is necessary to reduce the complexity of handling the finite difference representation of the governing equations and the associated boundary condition near the curved boundaries of the blade surfaces. This is best accomplished by introducing a coordinate transformation from the (m-ϕ-n) system of coordinate to a contracted body-fitted coordinate system. The overall effect of this transformation is to produce a square field in which the arbitrary blade shapes become straight and parallel. The development of such a coordinate transformation is presented in the next section.

2. BOUNDARY-FITTED COORDINATE SYSTEM

In all fields concerned with the numerical solution of partial differential equations, the physical region in which the solution is desired is overlayed with a grid. In constructing a grid over the blade-to-blade configuration of Fig. 4, the points on the blade surfaces do not generally correspond to grid points. Interpolation must therefore be used to determine the function values immediately adjacent to the boundary points, for the given boundary conditions. Moreover, if Neumann type boundary conditions are present, interpolation is also required to determine the boundary values themselves. Interpolation between grid points not coincident with the boundaries is particularly inaccurate in the case of field equations that produce large gradients in the vicinity of the boundaries [13]. This inaccuracy in representing the boundary conditions is known to impair the success of any numerical scheme in achieving an accurate convergent solution [15]. It is therefore desirable to use a coordinate system such that the problem boundaries lie along the coordinate directions. Such coordinate is commonly defined as a boundary-fitted coordinate system.

In this chapter, the available methods for developing boundary fitted coordinate systems for general shaped bodies are briefly discussed in the first section. The procedure used to transform the physical domain of Fig. 3, to a unit square using the boundary-fitted coordinate system is then outlined in section ii. The flow governing equations with their associated boundary conditions in the transformed domain are presented in the third section. The line integral method employed to obtain the pressure distribution within the flow field is covered in section iv.

i. Basic Transformation Methods

The importance of generating a boundary fitted coordinate system in viscous flow problems is evidenced by the fact that the only successful Navier-Stokes solutions to date have been for those bodies for which such coordinates is available. For

simple geometric shapes, it is usually possible to employ simple algebraic transformation to place one of the coordinates along the boundary surfaces. However, for more complex boundaries such as those involved in turbomachinery applications, it is extremely difficult if not impossible to use an analytical treatment to generate a boundary-fitted coordinate system. In these cases the boundary fitted coordinate system is generated numerically.

In reference [16], Stanitz takes the boundary-fitted coordinate to be the stream lines and equipotential lines that result from the solution of Laplace equation for the ideal two dimensional flow over the area of interest. Although this approach is straightforward and simple, it is strictly limited to two dimensions and is not particularly flexible in terms of coordinate spacing. A much more general method is to generate the boundary fitted coordinates by solving a pair of Poisson elliptic partial differential equations with Dirichlet boundary conditions. The boundary conditions specify one of the coordinates to be constant on each of the physical boundaries. A chosen distribution of the other coordinate is specified around the boundary contours. This procedure causes some coordinate lines to be coincident with each boundary of the physical domain regardless of its shape. The basic concept of such procedure has been employed in varied form by several investigators [18, 19,20]. Thompson [12] has extended this technique recently to be applied to multiconnected regions with any number of arbitrary shaped bodies. His method offers also the advantage of a provision for controlling the spacing of coordinate lines near any designated surface. These factors led to choose Thompson's approach to generate a boundary fitted coordinate system for the blade-to-blade domain of Fig. 3.

ii. Mathematical Formulation

Two transformations are employed in the present study to implement the generation of the boundary-fitted coordinate system for the blade-to-blade domain of Fig. 3. The first one is obtained by defining a stretched meridional coordinate, x, given by:

$$dx = \frac{dm}{r} \tag{26}$$

This coordinate stretching maps the physical space of Fig. 5a onto the domain shown in Fig. 5b with (x, ϕ) as coordinate system.

The second transformation [12] generates the boundary fitted coordinates ξ and η through the numerical solution of the following equations for $x(\xi,\eta)$ and $\phi(\xi,\eta)$.

$$\delta \frac{\partial^2 x}{\partial \xi^2} - 2\beta \frac{\partial^2 x}{\partial \xi \partial \eta} + \gamma \frac{\partial^2 x}{\partial \eta^2} = Q(\xi,\eta)$$

$$\delta \frac{\partial^2 \phi}{\partial \xi^2} - 2\beta \frac{\partial^2 \phi}{\partial \xi \partial \eta} + \gamma \frac{\partial^2 \phi}{\partial \eta^2} = P(\xi,\eta) \tag{27}$$

Subjected to the following boundary conditions:

$$x = g_1 (\xi,\eta_1) \qquad \text{on ABFG}$$

$$\phi = g_1 (\xi,\eta_1) \qquad \text{on ABFG}$$

$$x = g_2 (\xi,\eta_2) \qquad \text{on NMIH}$$

$$\phi = g_2 (\xi,\eta_2) \qquad \text{on NMIH} \tag{28}$$

where

$$\delta = \left(\frac{\partial x}{\partial \eta}\right)^2 + \left(\frac{\partial \phi}{\partial \eta}\right)^2$$

$$\beta = \frac{\partial x}{\partial \eta}\frac{\partial x}{\partial \xi} + \frac{\partial \phi}{\partial \xi}\frac{\partial \phi}{\partial \eta}$$

$$\gamma = \left(\frac{\partial x}{\partial \xi}\right)^2 + \left(\frac{\partial \phi}{\partial \xi}\right)^2 \qquad (29)$$

The functions Q and P in the above equations are appropriately chosen to provide control over the spacing of the coordinate lines in the field. On the other hand, the functions q_1, q_2, g_1 and g_2 are usually specified by the known shape of the contours ABFG and NMIH in the (x,ϕ) domain.

Mapping the region of interest in Fig. 5b in terms of the new boundary-fitted system of coordinates (ξ,η) yields a fixed square field in the final transformed domain as shown in Fig. 5c. Note that the blade surfaces in this transformed domain become straight and parallel. With this procedure the numerical solution of the flow equations developed in Section 1, is carried out on the fixed square field of Fig. 5c, using a uniform grid with no interpolation required regardless of the blades shape in the physical space. The transformation of the governing flow equations from the physical space to the transformed domain is outlined in the following section.

iii. Transformed Governing Equations

The general transformation from the physical space (m,ϕ) to the transformed field of (ξ,η) is given by equation (26) together with the following vector function:

$$\begin{bmatrix} \xi \\ \eta \end{bmatrix} = \begin{bmatrix} \xi(x,\phi) \\ \eta(x,\phi) \end{bmatrix} \qquad (30)$$

This vector function as well as its inverse transformation are defined once the (ξ,η) system has been obtained. Partial derivatives of any scalar function, f, are transformed utilizing the chain rule as follows:

$$\frac{\partial f}{\partial m} = \frac{1}{r}\left(\frac{\partial \phi}{\partial \eta}\frac{\partial f}{\partial \xi} - \frac{\partial \phi}{\partial \xi}\frac{\partial f}{\partial \eta}\right)/J$$

$$\frac{\partial f}{\partial \phi} = \left(\frac{\partial x}{\partial \xi}\frac{\partial f}{\partial \eta} - \frac{\partial x}{\partial \eta}\frac{\partial f}{\partial \xi}\right)/J \qquad (31)$$

where J is the Jacobian of transformation, given by:

$$J = \frac{\partial x}{\partial \xi}\frac{\partial \phi}{\partial \eta} - \frac{\partial x}{\partial \eta}\frac{\partial \phi}{\partial \xi}$$

Higher order derivatives as well as the derivatives normal to the different boundaries are presented in details in Appendix B. Using the expressions providing by the relations (31) and (B4) through (B10), the governing flow equations can be written as follows in terms of the new variables (ξ,η):

Vorticity Transport Equation

$$\frac{\partial}{\partial \xi}\left(\frac{\dot{M}}{b}\frac{\partial \psi}{\partial \eta}\omega\right) - \frac{\partial}{\partial \eta}\left(\frac{\dot{M}}{b}\frac{\partial \psi}{\partial \xi}\omega\right) - \frac{1}{J}\left[\delta\frac{\partial^2}{\partial \xi^2}(\mu_e\omega) - 2\beta\frac{\partial^2}{\partial \xi \partial \eta}(\mu_e\omega)\right.$$
$$\left. + \gamma\frac{\partial^2}{\partial \eta^2}(\mu_e\omega) + \sigma\frac{\partial}{\partial \eta}(\mu_e\omega) + \tau\frac{\partial}{\partial \xi}(\mu_e\omega)\right] + G_3 = 0 \qquad (32)$$

where the source term, G_3, is given by:

$$G_3 = \frac{\partial \rho}{\partial \xi}\frac{\partial W^2/2}{\partial \eta} - \frac{\partial \rho}{\partial \eta}\frac{\partial W^2/2}{\partial \xi} + 2\Omega\left[\frac{\partial}{\partial \xi}\left(\frac{\dot{M}}{b}\sin\alpha\frac{\partial \psi}{\partial \eta}\right) - \frac{\partial}{\partial \eta}\left(\frac{\dot{M}}{b}\sin\alpha\frac{\partial \psi}{\partial \xi}\right)\right]$$
$$+ \Omega^2 r^2 \sin\alpha\left(\frac{\partial x}{\partial \xi}\frac{\partial \rho}{\partial \eta} - \frac{\partial x}{\partial \eta}\frac{\partial \rho}{\partial \xi}\right) \qquad (32a)$$

And the coordinate transformation parameters σ and τ are given by the following expressions:

$$\sigma = \{\frac{\partial\phi}{\partial\xi}[\delta\ \frac{\partial^2 x}{\partial\xi^2} - 2\beta\ \frac{\partial^2 x}{\partial\xi\partial\phi} + \gamma\ \frac{\partial^2 x}{\partial\eta^2}] - \frac{\partial x}{\partial\xi}[\alpha\ \frac{\partial^2\phi}{\partial\xi^2} - 2\beta\ \frac{\partial^2\phi}{\partial\xi\partial\eta} + \gamma\ \frac{\partial^2\phi}{\partial\eta^2}]\}/J$$

$$\tau = \{\frac{\partial x}{\partial\eta}[\delta\ \frac{\partial^2\phi}{\partial\xi^2} - 2\beta\ \frac{\partial^2\phi}{\partial\xi\partial\eta} + \gamma\ \frac{\partial^2\phi}{\partial\eta^2}] - \frac{\partial\phi}{\partial\eta}[\alpha\ \frac{\partial^2 x}{\partial\xi^2} - 2\beta\ \frac{\partial^2 x}{\partial\xi\partial\phi} + \gamma\ \frac{\partial^2 x}{\partial\eta^2}]\}/J \qquad (32b)$$

It is not difficult to show that the right hand sides of the last two equations reduce to zero if a uniform mesh size is used along the ϕ direction. In this case, the coordinate system will be referred to as a non-contracting coordinate system.

Stream Function Equation

$$\delta\ \frac{\partial}{\partial\xi}\ (\frac{\dot{M}}{b\rho}\ \frac{\partial\psi}{\partial\xi}) - \beta\ \frac{\partial}{\partial\xi}\ (\frac{\dot{M}}{b\rho}\ \frac{\partial\psi}{\partial\eta}) - \beta\ \frac{\partial}{\partial\eta}\ (\frac{\dot{M}}{b\rho}\ \frac{\partial\psi}{\partial\xi}) + \gamma\ \frac{\partial}{\partial\eta}(\frac{\dot{M}}{b\rho}\ \frac{\partial\psi}{\partial\eta})$$

$$+ \frac{\dot{M}}{b\rho}\ (\sigma\ \frac{\partial\psi}{\partial\eta} + \tau\ \frac{\partial\psi}{\partial\zeta}) = -\ \omega\ r^2 J^2 \qquad (33)$$

Energy Equation

$$\frac{\dot{M}}{b}\ [\frac{\partial}{\partial\xi}\ (H\ \frac{\partial\psi}{\partial\eta}) - \frac{\partial}{\partial\eta}\ (H\ \frac{\partial\psi}{\partial\xi})] - \frac{1}{J}\ [\delta\ \frac{\partial}{\partial\xi}\ (\frac{\mu_e}{Pr}\ \frac{\partial H}{\partial\xi}) - \beta\ \frac{\partial}{\partial\xi}\ (\frac{\mu_e}{Pr}\ \frac{\partial H}{\partial\eta})$$

$$- \beta\ \frac{\partial}{\partial\eta}\ (\frac{\mu_e}{Pr}\ \frac{\partial H}{\partial\xi}) + \gamma\ \frac{\partial}{\partial\eta}\ (\frac{\mu_e}{Pr}\ \frac{\partial H}{\partial\eta}) + \frac{\mu_e}{Pr}\ (\sigma\ \frac{\partial H}{\partial\eta} + \tau\ \frac{\partial H}{\partial\xi})]$$

$$- \frac{D}{J} + G_4 = 0 \qquad (34)$$

where

$$G_4 = -\Omega \frac{\dot{M}}{b}\{\frac{\partial}{\partial\xi}[(W_\phi r + r^2\Omega)\frac{\partial\psi}{\partial\eta}] - \frac{\partial}{\partial\eta}[(W_\phi r + r^2\Omega)\frac{\partial\psi}{\partial\xi}]\}$$

$$+ \frac{\Omega}{J}\{\delta\frac{\partial}{\partial\xi}Q_3 - \beta\frac{\partial}{\partial\xi}Q_4 - \beta\frac{\partial}{\partial\eta}Q_3 + \gamma\frac{\partial}{\partial\eta}Q_4 + \sigma Q_4 + \tau Q_3\}$$

$$+ \frac{\dot{M}}{b\rho J}\{\delta\frac{\partial\psi}{\partial\xi}\frac{\partial(\mu_e\omega)}{\partial\xi} - \beta[\frac{\partial\psi}{\partial\xi}\frac{\partial(\mu_e\omega)}{\partial\eta} + \frac{\partial\psi}{\partial\eta}\frac{\partial(\mu_e\omega)}{\partial\xi}]$$

$$+ \gamma\frac{\partial\psi}{\partial\eta}\frac{\partial(\mu_e\omega)}{\partial\eta}\} + \frac{1}{J}(\delta\frac{\partial}{\partial\xi}Q_1 - \beta\frac{\partial}{\partial\xi}Q_2 - \beta\frac{\partial}{\partial\eta}Q_1$$

$$+ \gamma\frac{\partial}{\partial\eta}Q_2 + \sigma Q_2 + \tau Q_1) \qquad (34a)$$

and

$$Q_1 = \mu_e[\frac{1}{Pr}\frac{\partial W^2/2}{\partial\xi} - (\frac{1}{S_{CE}} - \frac{1}{Pr})\frac{\partial E}{\partial\xi}]$$

$$Q_2 = \mu_e[\frac{1}{Pr}\frac{\partial W^2/2}{\partial\eta} - (\frac{1}{S_{CE}} - \frac{1}{Pr})\frac{\partial E}{\partial\eta}]$$

$$Q_3 = \frac{\mu_e}{Pr}\frac{\partial}{\partial\xi}(W_\phi r + \frac{r^2\Omega}{2})$$

$$Q_4 = \frac{\mu_e}{Pr}\frac{\partial}{\partial\eta}(W_\phi r + \frac{r^2\Omega}{2}) \qquad (34b)$$

$$D = 2\mu_e\{(\frac{\partial\phi}{\partial\eta}\frac{\partial W_m}{\partial\xi} - \frac{\partial\phi}{\partial\xi}\frac{\partial W_m}{\partial\eta})^2 + (\frac{\partial x}{\partial\xi}\frac{\partial W_\phi}{\partial\eta} - \frac{\partial x}{\partial\eta}\frac{\partial W_\phi}{\partial\xi} + W_m\sin\alpha)^2\}$$

$$+ \mu_e\{(\frac{\partial\phi}{\partial\eta}\frac{\partial W_\phi}{\partial\xi} - \frac{\partial\phi}{\partial\xi}\frac{\partial W_\phi}{\partial\eta})^2 + (\frac{\partial x}{\partial\xi}\frac{\partial W_m}{\partial\eta} - \frac{\partial x}{\partial\eta}\frac{\partial W_m}{\partial\xi} - W_\phi\sin\alpha)^2\} \qquad (34c)$$

Turbulent Kinetic Energy Equation

$$\frac{\dot{M}}{b}\left[\frac{\partial}{\partial\xi}\left(E\,\frac{\partial\psi}{\partial\eta}\right)-\frac{\partial}{\partial\eta}\left(E\,\frac{\partial\psi}{\partial\xi}\right)\right]-\frac{1}{J}\left[\delta\,\frac{\partial}{\partial\xi}\left(\frac{\mu_e}{S_{CE}}\,\frac{\partial E}{\partial\xi}\right)-\beta\,\frac{\partial}{\partial\xi}\left(\frac{\mu_e}{S_{CE}}\,\frac{\partial E}{\partial\eta}\right)\right.$$

$$\left.-\beta\,\frac{\partial}{\partial\eta}\left(\frac{\mu_e}{S_{CE}}\,\frac{\partial E}{\partial\xi}\right)+\gamma\,\frac{\partial}{\partial\eta}\left(\frac{\mu_e}{S_{CE}}\,\frac{\partial E}{\partial\eta}\right)+\frac{\mu_e}{S_{CE}}\left(\sigma\,\frac{\partial E}{\partial\eta}+\tau\,\frac{\partial E}{\partial\eta}\right)\right]$$

$$-\frac{D}{J}+J\rho\,r^2\varepsilon=0 \qquad (35)$$

Dissipation Rate Equation

$$\frac{\dot{M}}{b}\left[\frac{\partial}{\partial\xi}\left(\varepsilon\,\frac{\partial\psi}{\partial\eta}\right)-\frac{\partial}{\partial\eta}\left(\varepsilon\,\frac{\partial\psi}{\partial\xi}\right)\right]-\frac{1}{J}\left[\delta\,\frac{\partial}{\partial\xi}\left(\frac{\mu_e}{S_{C\varepsilon}}\,\frac{\partial\varepsilon}{\partial\xi}\right)-\beta\,\frac{\partial}{\partial\xi}\left(\frac{\mu_e}{S_{C\varepsilon}}\,\frac{\partial\varepsilon}{\partial\eta}\right)\right.$$

$$\left.-\beta\,\frac{\partial}{\partial\eta}\left(\frac{\mu_e}{S_{C\varepsilon}}\,\frac{\partial\varepsilon}{\partial\xi}\right)+\gamma\,\frac{\partial}{\partial\eta}\left(\frac{\mu_e}{S_{C\varepsilon}}\,\frac{\partial\varepsilon}{\partial\eta}\right)+\frac{\mu_e}{S_{C\varepsilon}}\left(\sigma\,\frac{\partial\varepsilon}{\partial\eta}+\tau\,\frac{\partial\varepsilon}{\partial\eta}\right)\right.$$

$$-\bar{C}_1\,\frac{\varepsilon}{E}\,\frac{D}{J}+\bar{C}_2\rho\,\frac{\varepsilon^2}{E}\,J\,r^2=0 \qquad (36)$$

The above system of equations (32) - (36) are somewhat more complicated by the extra terms added by the transformation. The disadvantage of having these terms, however, is far outweighed by the computational advantages of the simple square flow region. In general, one can demonstrate that the transformed flow equations are still elliptic in spite of the appearance of the cross derivative terms $\frac{\partial}{\partial\xi}\,\frac{\partial}{\partial\eta}$. The numerical solution of these equations using a uniform rectangular gird in the (ξ,η) domain, provides the required distribution of the flow variables, ψ, ω, H, etc. in the physical space. The velocity components W_m, W_ϕ in the physical space can be related to the transformed ψ derivatives using equations (9) and (31) with the following result:

$$W_m=\frac{\dot{M}}{b\rho r}\left(\frac{\partial x}{\partial\xi}\,\frac{\partial\psi}{\partial\eta}-\frac{\partial x}{\partial\eta}\,\frac{\partial\psi}{\partial\xi}\right)/J$$

$$W_\phi=\frac{-\dot{M}}{b\rho r}\left(\frac{\partial\phi}{\partial\eta}\,\frac{\partial\psi}{\partial\xi}-\frac{\partial\phi}{\partial\xi}\,\frac{\partial\psi}{\partial\eta}\right)/J \qquad (37)$$

Boundary Conditions in the Transformed Domain

The boundary conditions for equations (32) to (34) are obtained by a proper transformation of the boundary conditions stated earlier in Section 1 to the new system of coordinate (ξ,η). This procedure yields the following relations.

a. The Upstream Boundary AN

$$\frac{\partial\psi}{\partial\xi} = \frac{1}{2\pi/Z}\left(\frac{\partial\phi}{\partial\xi} - \frac{\partial x}{\partial\xi}\tan\beta\right)_{inlet} \tag{38a}$$

$$\frac{\partial\psi}{\partial\eta} = 1$$

$$\omega = -(2\Omega\sin\alpha)_{inlet} \tag{38b}$$

$$H = (C_p T_{total})_{inlet} \tag{38c}$$

b. The Periodic Flow Boundaries AB, NM and FG, IH:

Figure 6 shows the grid ordering system in the transformed domain. The grid rows along $j = 1$ and $j = p$ correspond to the circumferential boundary of the blade-to-blade passage AB, NM, and FG, IH. The grid rows along $j = -1$ and $j = p+1$ are exterior to the blade rows and are reserved in the computational procedure for the enforcement of the periodicity condition. Accordingly, along $j = 1$ and $j = p$, the following conditions apply

$$\psi_{i,-1} = \psi_{i,p-1}^{-1}\ , \quad \psi_{i,1} = \psi_{i,p}^{-1}\ , \quad \psi_{i,2} = \psi_{i,p+1}^{-1} \tag{39a}$$

$$\omega_{i,-1} = \omega_{i,p-1}\ , \quad \omega_{i,1} = \omega_{i,p}\ , \quad \omega_{i,2} = \omega_{i,p+1} \tag{39b}$$

$$H_{i,-1} = H_{i,p-1}\ , \quad H_{i,1} = H_{i,p}\ , \quad H_{i,2} = H_{i,p+1} \tag{39c}$$

where i, is the finite difference grid counter in the ξ direction. Similar relations are used for the grid points along FG and IH.

c. The Blade Surfaces MI and BF:

Laminar flow case

$$\psi = 0 \quad \text{(Along MI)} \tag{40a}$$

$$\psi = 1 \quad \text{(Along BF)} \tag{40b}$$

$$\omega_w = - \left[A(\psi_{w+1} - \psi_w) + \frac{1}{2}\,\omega_{w+1} + B\right] \cdot C \tag{40c}$$

(For both Mi, BF)

$$H_w = C_p\, t_w + \frac{\Omega^2 r^2}{2} \qquad \text{(for both MI, BF)} \tag{40d}$$

where

$$A = \frac{3}{\Delta\eta^2}\left[\frac{\dot{M}}{b\rho}\,\frac{\gamma}{J^2 r^2}\right]_w$$

$$B = \left[\frac{\dot{M}}{b\rho}\,\frac{\beta}{J^2 r^2}\,\Delta\eta\,\frac{\partial}{\partial\xi}\left(\frac{\omega J^2 r^2}{\gamma \dot{M}/b\rho}\right)\right]_w \tag{40e}$$

$$C = \ldots/\left\{1 - \frac{\Delta\eta}{2\gamma}\left[\frac{\partial\gamma}{\partial\eta} + \frac{2\gamma b\rho}{\dot{M}}\,\frac{\partial}{\partial\eta}\left(\frac{\dot{M}}{b\rho}\right) - \frac{\beta b\rho}{\dot{M}}\,\frac{\partial}{\partial\xi}\left(\frac{\dot{M}}{b\rho}\right) + \sigma\right]\right\}_w$$

In the above equations the subscript (w) denotes a blade boundary point and the subscript (w+1) denotes a point in the flow field at a distance $\Delta\eta$ away from w. The vorticity boundary condition given by equation (40c) is derived using a Taylor's series expansion for the stream function about the blade surface, the boundary conditions given by equation (23) and the stream function equation (33). The formulation of the vorticity boundary condition

as given by this equation is second order accurate and allows implicit treatment in the solution technique.

d. The Downstream Boundary GH:

$$\frac{\partial \psi}{\partial \xi} = \frac{1}{2\pi/Z} \left(\frac{\partial \phi}{\partial \xi} - \frac{\partial x}{\partial \xi} \tan\beta\right)_{exit} \tag{41a}$$

$$\omega = - \left[2\Omega \sin\alpha\right]_{exit} \tag{41b}$$

$$\frac{\partial H}{\partial \xi} = 0 \tag{41c}$$

iv. Pressure Distribution

In the stream function-vorticity formulation of the flow equation, the pressure does not appear explicitly in the problem. Therefore, indirect methods must be used to evaluate the pressure distribution through the flow field. An accurate approach consists of forming a Poisson equation for the pressure using equations (7) and (8). The Poisson equation is then solved to determine the pressure, subject to Neumann-type boundary conditions provided by the momentum equations. A variety of numerical procedures for this type of solution are given in reference [13]. The principal problem encountered with such an approach is that the Neumann boundary conditions should be formulated carefully such that they are compatible with the source term in Poisson equation. Because of the truncation errors, the boundary values fail usually to meet this constraint, resulting in a slow divergence of the numerical solution. An alternative approach to obtain a pressure distribution is to perform a line integral for the pressure gradients $\frac{\partial p}{\partial \xi}$, $\frac{\partial p}{\partial \eta}$ along a contour in the flow field. This approach usually yields reasonably accurate values for the pressure along the surface of a smooth body without sharp corners as is the case in the present flow configuration.

The pressure gradients $\frac{\partial p}{\partial \xi}$ and $\frac{\partial p}{\partial \eta}$ are related to the velocity components W_m, W_ϕ, the vorticity ω and their derivatives by the following relations:

$$\frac{\partial p}{\partial \xi} = \frac{1}{J}\left[\beta \frac{\partial}{\partial \xi}(\mu_e \omega) - \gamma \frac{\partial}{\partial \eta}(\mu_e \omega)\right] - \rho\{W_m \frac{\partial W_m}{\partial \xi} + W_\phi \frac{\partial W_\phi}{\partial \xi}$$

$$+ \omega r(W_m \frac{\partial \phi}{\partial \xi} - W_\phi \frac{\partial x}{\partial \xi}) - (\Omega^2 r^2 \sin\alpha + 2\Omega W_\phi r \sin\alpha) \frac{\partial x}{\partial \xi}$$

$$+ 2\Omega r W_m \sin\alpha \frac{\partial \phi}{\partial \xi}\} + \frac{4}{3}\frac{\partial F}{\partial \xi} \qquad (42a)$$

and

$$\frac{\partial p}{\partial \eta} = \frac{1}{J}\left[\delta \frac{\partial(\mu_e \omega)}{\partial \xi} - \beta \frac{\partial}{\partial \eta}(\mu_e \omega)\right] - \rho\{W_m \frac{\partial W_m}{\partial \eta} + W_\phi \frac{\partial W_\phi}{\partial \eta}$$

$$+ \omega r(W_m \frac{\partial \phi}{\partial \eta} - W_\phi \frac{\partial x}{\partial \eta}) - (\Omega^2 r^2 \sin\alpha + 2\Omega r W_\phi \sin\alpha)\frac{\partial x}{\partial \eta}$$

$$+ 2\Omega r W_m \sin\alpha \frac{\partial \phi}{\partial \eta}\} + \frac{4}{3}\frac{\partial F}{\partial \eta} \qquad (42b)$$

where

$$F = \frac{\mu_e}{r}\left[W_m \sin\alpha + \frac{1}{J}\left(\frac{\partial \phi}{\partial \eta}\frac{\partial W_m}{\partial \xi} - \frac{\partial \phi}{\partial \xi}\frac{\partial W_m}{\partial \eta} + \frac{\partial x}{\partial \xi}\frac{\partial W_\phi}{\partial \eta} - \frac{\partial x}{\partial \eta}\frac{\partial W_\phi}{\partial \xi}\right)\right] \qquad (42c)$$

In deriving these relations, use has been made of the momentum equations (7) and (8), together with the transformation relations (1b) through (10b), as well as the definition of ω given by equation (14).

Once a solution to the transformed flow equations has been obtained, the right hand side of equation (42a) and (42b) can be evaluated using second order central difference for the ξ and η derivatives. From a mathematical view point, equations (42a) and (42b) represent algebraic expressions for the various pressure gradients. The pressure distribution over the whole field can therefore be obtained by performing a line integral for these algebraic expressions. Starting from the upstream inlet boundary (AN) of Figure 6 where the pressure level is known, the pressure distribution along the mid channel line (L-L) is obtained using the following integration formula:

$$\int_{i-1}^{i} \frac{\partial p}{\partial \xi} d\xi = - p_{i-1} + \frac{1}{2} \left[\left(\frac{\partial p}{\partial \xi}\right)_{i-1} + \left(\frac{\partial p}{\partial \xi}\right)_{i} \right] \cdot (\xi_i - \xi_{i-1}) \qquad (43)$$

A similar expression is used to integrate equation (43) in the η direction. In this case the integration starts with the predicted pressure values along the mid channel line (L-L) and proceeds towards both the suction and pressure surface of the blades.

3. SOLUTION PROCEDURE

The flow governing equations introduced earlier as equations (32) through (34) comprise a system of coupled nonlinear elliptic partial differential equations that must be solved, subject to the boundary conditions (38) - (41), to provide the details of the flow pattern within the blade-to-blade channels. Since the flow equations are not tractable to analytical solutions, a numerical solution which is based on the finite difference method is used. The following simplifications are made in order to reduce the complexity of handling the numerics of the problem. First, the flow is considered to be incompressible. This decouples the energy equation from the momentum equations. Thus, it is possible to solve the ψ and ω equations to obtain the velocity distribution which are then used in the energy equation to determine the enthalpy distribution throughout the flow field. This assumption is mandatory in order to develop a method of solution which could be later expanded to take into account the density variation within the flow. Second, a non-contracting body fitted coordinate system is employed during the numerical solutions. Consequently, all first order terms containing the transformation parameters σ, τ, in equations (32) - (34) vanished as pointed out in Section 2. It should also be remarked that using non-contracting body fitted coordinates implies that the spacing of the coordinate lines, in ϕ direction, in the physical domain, is uniform.

Before writing the governing equations in finite difference form, it is found more convenient to express the flow variables in the following dimensionless form:

$$\omega^* = \frac{\omega r_t}{(W_m)_o}, \qquad H^* = \frac{H}{(W_m^2)_o}, \qquad r^* = \frac{r}{r_t}, \qquad b^* = \frac{b}{b_t},$$

$$Re = (W_m)_o \frac{\rho r_t}{\mu_e}, \qquad R_o = \frac{\rho \Omega r_t^2}{\mu_e} \tag{44}$$

Where the subscripts o, t denote the condition at the upstream boundaries (A-N) and M-B) respectively (see Fig. 3). Using the above equation, one can express the flow governing equations in nondimensional for as follows:

Stream Function Equation

$$\frac{r_o}{r_t}\frac{b_o}{b_t}\frac{2\pi}{z}\left\{\alpha \frac{\partial}{\partial \xi}\left(\frac{1}{b^*}\frac{\partial \psi}{\partial \xi}\right) + \gamma \frac{\partial}{\partial \eta}\left(\frac{1}{b^*}\frac{\partial \psi}{\partial \eta}\right) - \beta \frac{\partial}{\partial \xi}\left(\frac{1}{b^*}\frac{\partial \psi}{\partial \eta}\right)\right.$$

$$\left. - \beta \frac{\partial}{\partial \eta}\left(\frac{1}{b^*}\frac{\partial \psi}{\partial \xi}\right)\right\} = - \omega^* r^{*2} J^2 \tag{45}$$

Vorticity Transport Equation

$$J\left[\frac{\partial}{\partial \xi}\left(\frac{\omega^*}{b^*}\frac{\partial \psi}{\partial \eta}\right) - \frac{\partial}{\partial \eta}\left(\frac{\omega^*}{b^*}\frac{\partial \psi}{\partial \xi}\right)\right] + 2J \frac{R_o}{Re}\left[\frac{\partial}{\partial \xi}\left(\frac{\sin\alpha}{b^*}\frac{\partial \psi}{\partial \eta}\right)\right.$$

$$\left. - \frac{\partial}{\partial \eta}\left(\frac{\sin\alpha}{b^*}\frac{\partial \psi}{\partial \xi}\right)\right] - \frac{r_t}{r_o}\frac{b_t}{b_o}\frac{z}{2\pi}\left[\delta \frac{\partial^2}{\partial \xi^2}\left(\frac{\omega^*}{Re}\right) + \gamma \frac{\partial^2}{\partial \eta^2}\left(\frac{\omega^*}{Re}\right)\right.$$

$$\left. - 2\beta \frac{\partial^2}{\partial \xi \partial \eta}\left(\frac{\omega^*}{Re}\right)\right] = 0 \tag{46}$$

Energy Equation

$$J \frac{b_o^*}{b^*} \left[\frac{\partial}{\partial \xi} \left(H^* \frac{\partial \psi}{\partial \eta}\right) - \frac{\partial}{\partial \eta} \left(H^* \frac{\partial \psi}{\partial \xi}\right)\right] - \frac{r_t}{r_o} \frac{Z}{2\pi} \left[\delta \frac{\partial}{\partial \xi} \left(\frac{1}{Re} \frac{1}{Pr} \frac{\partial H^*}{\partial \xi}\right)\right.$$

$$- \beta \frac{\partial}{\partial \xi} \left(\frac{1}{Re} \frac{1}{Pr} \frac{\partial H^*}{\partial \eta}\right) - \beta \frac{\partial}{\partial \eta} \left(\frac{1}{Re} \frac{1}{Pr} \frac{\partial H^*}{\partial \xi}\right) + \gamma \frac{\partial}{\partial \eta} \left(\frac{1}{Re} \frac{1}{Pr} \frac{\partial H}{\partial \eta}\right)$$

$$\left. - D^* + G_4^* = 0 \right. \qquad (47)$$

where z is the number of blades, D^* and G_4^* are the nondimensional equivalent of the source terms D, G_4 in equations (34a) and (34b).

Numerical Solution

The derivations of the finite difference equations is followed by a description of the iterative procedure used to obtain the numerical solution.

The Finite Difference Equations

A noteworthy comment is to be made before expressing equations (45) - (47) totally in a finite difference form. This relates to the effective handling of the first order convective terms in the above equations. As pointed out by Roache [13], these terms can destroy the diagonal dominance of the matrix of the finite difference equations to be solved at high Reynolds numbers. This in turn causes inversion instabilities that produce spatial oscillation "wiggles" in the final solution for the flow variables. To eliminate these instabilities, a windward difference technique is used to model the longitudinal convective terms. Thus, when the local value of the ξ component of velocity is positive, the convective terms including $\frac{\partial \omega^*}{\partial \xi}$ or $\frac{\partial H^*}{\partial \xi}$ are evaluated with a backward difference. On the other hand, when the velocity is negative, a forward difference approximation is used for either $\frac{\partial \omega^*}{\partial \xi}$ or $\frac{\partial H^*}{\partial \xi}$. In a similar fashion, the windward differencing technique is used to control the difference representation of the normal convective terms containing $\frac{\partial \omega^*}{\partial \eta}$ and $\frac{\partial H^*}{\partial \eta}$ in equations (46) and (47).

Referring now to Fig. 6, it can be shown that the finite difference representation of equations (45) - (47) may be written as

$$\psi_{i,j} = A_1 \psi_{i+1,j} + A_2 \psi_{i-1,j} + A_3 \psi_{i,j+1} + A_4 \psi_{i,j-1} + A_5 \quad (48)$$

and

$$\omega^*_{i,j} = B_1 \omega^*_{1+1,j} + B_2 \omega^*_{i-1,} + B_3 \omega^*_{i,j+1} + B_4 \omega^*_{i,j-1} + B_5 \quad (49)$$

and

$$H^*_{i,j} = C_1 H^*_{i+1,j} + C_2 H^*_{i-1,j} + C_3 H^*_{i,j+1} + C_4 H^*_{i,j-1} + C_5 \quad (50)$$

Where the coefficients A_5, B_5 and C_5, in the above equations serve as the explicitly known source terms. The value of these coefficients as well as the cofficients A_1 through A_4, B_1 through B_4, and D_1 through D_4, are given in Table 2.

Iterative Procedure

For the numerical solution of our system of coupled finite difference equations (48) - (50), a wide variety of classical matrix iteration techniques are available. The point SOR method of solution has generally been acknowledged as being the best of these iterative techniques, because of its effectiveness and simplicity of application. Within the category of the point iterative method, there is a choice of alternate methods. In the present report, the Gauss-Seidel method is used, for it is known to yield more rapid convergence solution and places less demands on computer storage.

TABLE 2. COEFFICIENTS OF THE FINITE DIFFERENCE EQUATIONS†

$$A_1 = 2\delta\ \Delta\eta/\Delta\xi/A_o/(b^*_{i+1} + b^*_i)$$

$$A_2 = 2\delta\Delta\eta/\Delta\xi/A_o/(b^*_{i-1} + b^*_i)$$

$$A_3 = \gamma\ \Delta\xi/\Delta\eta/A_o/b^*_i$$

$$A_4 = \gamma\ \Delta\xi/\Delta\eta/A_o/b^*_i$$

$$A_5 = \Delta\xi\ \Delta\eta\ [\frac{r_t}{r_o}\frac{b_t}{b_o}\omega^* R^2 J^2\ z/2\pi - \underline{\beta}\ \frac{\partial}{\partial\xi}(\frac{1}{b^*}\frac{\partial\psi}{\partial\eta}) - \underline{\beta}\ \frac{\partial}{\partial\eta}\ (\frac{1}{b^*}\frac{\partial\psi}{\partial\xi})]/A_o$$

where

$$A_o = A_1 + A_2 + A_3 + A_4$$

† All unsubscript quantities in this table are evaluated at the grid node (i,j). Note that the stream channel thickness b^*_i is constant for all j.

TABLE 2 - CONTINUED

$$B_1 = [B_{11} + B_{12}\, b^*_{i+1}/(\tilde{Re})_{i+1,j}]\, b^*_i/b^*_{i+1} \quad , \qquad \tilde{Re} = \frac{r_o}{r_t}\frac{b_o}{b_t}\frac{2\pi}{z}\, Re$$

$$B_2 = [B_{21} + B_{22}\, b^*_{i-1}/(\tilde{Re})_{i-1,j}]\, b^*_i/b^*_{i-1}$$

$$B_3 = [B_{31} + B_{32}\, b^*_i/(\tilde{Re})_{i,j+1}]\, b^*_i/b^*_{i+1}$$

$$B_4 = B_{41} + B_{42}\, b^*_i/(\tilde{Re}_{i,j-1})$$

where

$$B_{11} = J(\psi_{11} + |\psi_{11}|)/8B_o$$

$$B_{12} = \delta\, \Delta\eta/\Delta\xi/B_o$$

$$B_{21} = J(\psi_{22} + |\psi_{22}|)/8B_o$$

$$B_{22} = \delta\, \Delta\eta/\Delta\xi/B_o$$

$$B_{31} = J(\psi_{33} + |\psi_{33}|)/8B_o$$

$$B_{32} = \gamma\, \Delta\xi/\Delta\eta/B_o$$

TABLE 2 - CONTINUED

$$B_{41} = J(\psi_{44} + |\psi_{44}|)/8B_o$$

$$B_{42} = \gamma\ \Delta\xi/\Delta\eta/B_o$$

$$B_5 = -\ 2\ \Delta\xi\ \Delta\eta\ b^*[\underline{\beta}\ \frac{\partial^2}{\partial\xi\ \partial\eta}\ (\frac{\omega^*}{\tilde{Re}}) + J\ \frac{R_o}{Re}\ \frac{\partial}{\partial\xi}\ (\frac{\sin\alpha}{b^*}\ \frac{\partial\psi}{\partial\eta}) + \frac{\partial}{\partial\eta}\ (\frac{\sin\alpha}{b^*}\ \frac{\partial\psi}{\partial\xi})]/B_o$$

$$B_o = B_{11} + B_{21} + B_{31} + B_{41} + (B_{12} + B_{22} + B_{32} + B_{42})\ b^*/\tilde{Re}$$

$$\psi_{11} = \psi_{i+1,j-1} + \psi_{i,j-1} - \psi_{i+1,j+1} - \psi_{i,j+1}$$

$$\psi_{22} = \psi_{i-1,j+1} + \psi_{i,j+1} - \psi_{i-1,j-1} - \psi_{i,j-1}$$

$$\psi_{33} = \psi_{i+1,j+1} + \psi_{i+1,j} - \psi_{i-1,j+1} - \psi_{i-1,j}$$

$$\psi_{44} = \psi_{i-1,j-1} + \psi_{i-1,j} - \psi_{i+1,j-1} - \psi_{i+1,j+1}$$

TABLE 2 - CONTINUED*

$$C_1 = (C_{11} + C_{12})/C_o$$

$$C_2 = (C_{21} + C_{22})/C_o$$

$$C_3 = (C_{31} + C_{32})/C_o$$

$$C_4 = (C_{41} + C_{42})/C_o$$

where

$$C_{11} = J\ b_o^*\ (\psi_{11} + |\psi_{11}|)/8b^*$$

$$C_{12} = \delta\ \Delta\eta/\Delta\xi/Pr/[(\tilde{Re})_{i+1,j} + (\tilde{Re})_{i,j}]$$

$$C_{21} = J\ b_o^*\ (\psi_{22} + |\psi_{22}|)/8b^*$$

$$C_{22} = \delta\ \Delta\eta/\Delta\xi/Pr/[(\tilde{Re})_{i-1,j} + (\tilde{Re})_{i,j}]$$

* The Prandtl Number is assumed to be constant in this table.

In using the Gauss-Seidel method, two cycles of iterations are required to obtain a complete solution to equations (48) - (50). The first cycle consists of the iterative solution of the stream function and vorticity equations. When a converged solution is reached for these two equations, the energy equation is then solved in the final cycle. During the first cycle of iterations, a successive over-relaxation, using an optimum over-relaxation factor, R_f, is used. The iterative procedure is given by

$$\theta = R_f \, \theta^{n+1} + (1 - R_f) \, \theta^n \tag{51}$$

where θ denotes a general flow property and includes ψ and ω. The superscripts (n+1), and n represent an iteration counter.

For the final cycle of iterations it is found that using an under relaxation factor, U, improved the convergence characteristics. The under relaxation relation used is

$$H = U \, H^{n+1} + (1 - U) \, H^n \tag{52}$$

In the present solution the optimum values for the different relaxation factors are determined by trial and error.

Boundary Conditions in the Iterative Scheme

The general recursive formulae for the iterative solution as given by equations (48) - (50) are only applied at the interior nodes of the flow domain. Near the various boundaries equations similar to (38) - (41) are used. Along the upstream and downstream boundaries, equations (38) and (41) are introduced in the solution procedure in a straightforward manner with minimum computational effort. However, along the periodic boundaries AB, NM, FG and IH, the boundary conditions provided by equation (39) have a unique feature. Specifically, neither the boundary values nor the derivatives of any of the flow properties are specified apriori along these boundaries. The only information supplied by equation (39) are the equality of the function values and

their derivatives at every two corresponding points. Therefore, a special approach is required to determine the values of the dependent variables ψ, ω, and H, along the periodic boundaries. The approach to be taken here relies on a modified evaluation of the governing equation for each flow property to determine the boundary condition for the flow property in question. The modification is introduced in an attempt to insure that equation (39) holds, that is to satisfy the periodicity condition. The numerical procedure is as follows.

Let the generalized finite-difference form of any of the flow governing equations (45) - (47) be represented by, (see Fig. 6 for subscript notation):

$$\theta_{i,j} = a_1\,\theta_{i+1,j} + a_2\,\theta_{i-1,j} + a_3\,\theta_{i,j+1} + a_4\,\theta_{i,j-1} + a_5 \tag{53}$$

where θ denotes a general flow property (ψ, ω, and H). The coefficients a_1 through a_5 depend on the particular equation used, and are obtained by a proper combination of the coefficients A_1 through C_5 given in Table 2. For the grid points along the boundary AB of Fig. 6, the above equation is modified, using the periodic boundary conditions given by equation (39) to the following form:

$$\theta_{i,1} = a_1\,\theta_{i+1,1} + a_2\,\theta_{i-1,1} + a_3\,\theta_{i,2} + a_4\,\theta_{i,p-1} + a_5 + \chi_1 \tag{54}$$

where $\chi_1 = 0$ for ω and H;

$\chi_1 = -a_4$ for ψ. (54a)

The points along NM are not part of the solution regions, since the value of the dependent variables at each of them is just equal to the corresponding point along AB. The equation for the first mesh line below NM must be modified by substituting the periodicity condition given by equation (39) into equation (53).

$$\theta_{i,p-1} = a_1\,\theta_{i+1,p-1} + a_2\,\theta_{i-1,p-1} + a_3\,\theta_{i,1} + a_4\,\theta_{i,p-2} + a_5 + \chi_2 \qquad (55)$$

where $\chi_2 = 0$ for ω and H;

$\chi_2 = a_3$ for ψ . (55a)

A similar approach can be applied along the other boundaries (FG and IH) where a periodic condition exists.

4. RESULTS AND DISCUSSION

The equations formulated in Section 2 are programmed for numerical solution using the finite difference technique discussed in Section 3. The program is arranged to handle general flow within turbomachinery, which may be of the axial, radial or mixed flow type. In general, the program requires as an input the configuration of the stream channel annulus S_1, the inlet flow conditions, the rotational speed of the machine, and the blade geometry. Recalling that all the flow calculations are carried out in the unit square of the transformed domain, therefore the blade input geometry is supplied to the program in the form of the transformation parameters δ, β, γ and J. As pointed out in Section 2, these parameters may be specified for any blade geometry using Thompson code for the automatic numerical generation of boundary fitted coordinate system [12].

The program output consists of the distribution of the stream function, the vorticity, and the static pressures within the blade passages. The variation of meridional and tangential velocity components from blade-to-blade and from the inlet of the machine to its exit are also generated. In cases where blade cooling is considered, the program has the capability to generate the temperature distribution within the blade passages. In order to keep the computer time within reasonable limits, (usually less than 5 minutes on an AMDAHL 470), the flow domain has been divided, for all calculations, into 30 step sizes in η direction and 40 in the ζ direction, with the greater number of nodes distributed in the meridional direction.

Five flow cases are investigated using the developed program. The main purpose was to check the accuracy of the present method of analysis in predicting the actual flow behavior within turbomachine channels. The accuracy of the method was confirmed by a comparison with available experimental data. Four of those investigated cases were concerned with inward flow situations, while the fifth one dealt with an outward flow case. In all cases investigated, the flow was considered to be incompressible and having a constant effective viscosity, μ_e. The blade surfaces are assumed to be adiabatic with no heat sources or sinks.

Inward Flow Cases

These flow cases are those of a radial inflow turbine whose rotor consists of eight radial straight blades. A full description of the rotor geometry is given in Fig. 7. The primary reason for the selection of this specific rotor is that a substantial amount of experimental data is available for it (reference [20]). Thus, besides providing a basis for comparison with the theoretical predictions, the experimental evidence is used to show avenues for future development in the present method of analysis.

The flow patterns are investigated on a blade-to-blade stream channel, S_1, located midway the passage depth of the rotor as

shown in Fig. 7. The results are presented over a wide range of operating conditions, which are summarized in Table 3. The coordinate system used in the solution is illustrated in Fig. 8. The results presented include stream function contour plots, velocity profiles across the rotor passages together with some information concerning the pressure distribution within these passages.

The streamline contours for the four inward flow cases of Table 3 are shown in Figs. 9a and 9b. The streamlines are plotted for the region between a pair of blades, represented by the heavy thick lines. The streamlines are designated by a stream function ratio ψ/ψ_{total} such that the value on a streamline indicates the ratio of flow through the passage between the streamline and the pressure surface of the blade. Thus, for the given channel configuration, the streamline spacing is indicative of the velocity relative to the rotor, with close spacing indicating high velocities and wide spacing indicating low velocities. For the operating conditions corresponding to case 1, as shown in Fig. 9a, it is observed that a recirculating eddy began to form near the pressure surface of the blades. As the rotating speed increases, the recirculating zone grows much larger, as shown for case 3 in Fig. 9b. The relative velocity near the suction side of the blades increases in the later case. This effect may be attributed to the fact that the effective sectional area of the rotor decreases with the growth of the recirculating zone. Since large recirculatory zones cause higher losses in total pressure, it is desirable to avoid them through efficient rotor design and proper selection of the oeprating conditions. From the inspection of Fig. 9, it can be concluded that the size of the recirculating eddy depends upon the relative magnitude of the flow rate $(\dot{M}\sqrt{T_t}/p_t)$ and on the rotor speed, $N/\sqrt{T_t}$. These zones generally can be reduced by increasing the mass flow rate and/or decreasing the rotor tip speed.

The most remarkable feature of the present results is the good agreement obtained between the predicted flow behavior and the experimental evidence taken from reference [20]. In all

cases studied, the size and the extent to which the recirculating zone grows compares favorably well with the experimental data, as indicated in Fig. 9.

Figures 10a and 10b show the predicted meridional velocity distribution across the blade passages at three different radial locations. These locations are selected to correspond to a radius of 23.2, 15 and 6.8 cms, respectively. The dotted line shown on each figure represents the velocity distribution for an inviscid solution. The results of the viscous flow analysis show a large variation in the meridional velocity profiles as the flow travels downstream. The profile distribution, at stations located away from the turbine inlet, indicate that regions of high meridional velocities are shifted towards the blades suction surface as shown in Figs. 10a and 10b. While, regions of high relative meridional velocities are observed to exist near the blades pressure surface at subsequent downstream stations. Compared with the viscous calculations, the inviscid flow solution predicts a completely different flow behavior, in this respect. Moreover, in some flow situations where severe changes take place near the rotor tip as in case 4 in Fig. 10b, the inviscid flow solution fails completely even in predicting the flow characteristics. All these factors, in addition to the existance of reversed flow regions near the blades pressure surface make it clear why the inviscid solutions always fail to produce a realistic prediction of boundary layer characteristic parameters in rotating machines when used in conjunction with standard boundary layer analysis.

Figures 11a,b,c show the pressure variation between blades at four radial locations corresponding to radius, r = 13.1, 16.3, 19.5 and 22.7 cms. The static pressure, p, is plotted in these figures using the nondimensional quantity, $C_p = (p_1-p)/\frac{\rho_1 \Omega^2 r_{tip}^2}{2g}$, where p_1, ρ_1 are the mean static pressure and density at rotor inlet respectively. The experimental measurements of reference [20]

are also shown in the same figures. As with the stream function and velocity results, the present method of analysis provides a good prediction of the pressure distribution over a wide range of operating conditions. On the whole, the value of C_p is observed to be larger on the suction side of the blades and decreases near the pressure surface, with smaller changes in C_p values at higher rotational speeds. In the region lying between the center of the passage and the pressure surface, the C_p values become smaller as the rotational speeds decrease. These observations imply that the static pressure drop from the rotor inlet increases with increased rotational speed. Near the suction surface, the pressure drop increases with the decrease of rotational speed. Such a tendency is remarkable, particularly near the rotor inlet.

Some comments might also be made concerning the discrepancies observed between the predicted and experimental values of pressure distribution in case 4 near the rotor exit (i.e. at r = 13.1). As reported in the experimental work of reference [20], the operating conditions for this case cause the flow to be heavily separated†. The existance of large separation zone within the rotor is believed to modify the channel shape in such a way as if the zone acts as a pseudo blade. This in turn affects the pressure distribution in the manner shown in Fig. 11c. Therefore, it appears that in order to deal with flow cases where heavy separation is encountered within the rotor channel, one has to incorporate a zonal model for such separation in the present method of analysis. Such development in the method of solution is undoubtably essential for further use of this method of analysis in aerodynamic improvement and performance prediction of turbomachines.

---

† It is to be noted that this type of separation is not a regular two dimensional one, but rather a three dimensional type.

Flow in Radial Compressor

The capability of the present method to analyze the flow in diffusion cascades is examined by studying the flow behavior within the rotor of a radial bladed compressor. The rotor profile is shown in Fig. 12. The rotor has 12 straight radial blades. The blade-to-blade shape in the physical domain as well as the coordinate system used in the solution are shown in Fig. 13. Additional summary data for the solution appear in Table 3 (as case number 5). A typical distribution of the flow properties on the blade-to-blade computational surface, S_1, of Fig. 12 are calculated and the corresponding results are calculated and the corresponding results are presented in Figs. 14 and 15.

Figure 14 shows a comparison between the predicted streamline contours and those determined experimentally in reference [21]. The experimental evidence was obtained by tracing photographs of streak lines from the rotor segments under the same operating conditions reported here. Good agreement is generally observed and it should be particularly noted that the shape and the size of the recirculating eddy compare favorably well in both cases.

The predicted meridional velocity profiles across the rotor passage at three different radial locations are illustrated in Fig. 15. Shown also in the same figure, the calculated velocity distribution using an inviscid blade-to-blade analysis. The inviscid solution, although showing the existance of negative flow regions as exemplified in Fig. 15b, over estimates the size of the recirculating eddy noted in Fig. 14. This overestimation is supported by the existance of large negative meridional velocities near the blade suction surface. In an actual case, boundary layer phenomena are expected to reduce the effective flow area of the passage, thus increasing the volume flow rate per unit area through the effective area and thereby reducing the size of the eddy. This is exactly the same result obtained using the present viscous flow solution.

TABLE 3. PARAMETER FOR THE NUMERICAL SOLUTIONS*

Case No.	Designation	Corrected Weight Flow $\dot{W}\sqrt{T_t}/p_t$	Corrected Speed** $N/\sqrt{T_t}$	Tip Speed $U_{tip} = \Omega r_{tip}$ m/sec	Inlet Flow Angle, β_{in}, Along the Boundary, AN, degrees	Exit Flow Angle, β_{exit}, Along the Boundary, HG, degrees	Reynolds Number $\left(\frac{\rho N r_{tip}}{\mu_e}\right)_{inlet}$	Inlet Total Temperature, T_t °K	Inlet Total Pressure, p_t, (Kg/m^2)	Remarks† Computation Time (sec)
1	Inward-Flow Turbine	0.0011	87.9	39.3	72.27°	33.7°	1.175×10^5	288	10540	117
2	Inward-Flow Turbine	0.0012	87.3	39.3	74.25°	37.7°	1.208×10^5	288	10600	121
3	Inward-Flow Turbine	0.0012	116.6	52.0	79.77°	10.5°	1.219×10^5	288	10670	106
4	Inward-Flow Turbine	0.0012	145.6	65.4	81.28	6.3°	1.275×10^5	288	10750	119
5	Compressor	0.00343	589.25	261.8	44.5°	81.2°	1.370×10^5	288	10330	130

* In all cases studied, the upstream boundary AN of Figures 8 and 13 is located at radius ratio r/r_{tip} of 1.35, while the downstream boundary HG is located at radius ratio r/r_{tip} of 0.254.

** N designates the rotational speed (r.p.m.)

† For all cases, the blade surfaces are considered to be adiabatic and the flow is assumed to be laminar with constant viscosity, μ_e.

On the whole, the present method of analysis provides a good prediction of the actual flow behavior within the passage of turbomachine rotors. The preservation of the ellipticity of the flow problem is believed to be the major element that results in such good prediction. The ellipticity is preserved through the consideration of all the diffusion terms of the governing equations during the solution procedures. The method of analysis proves also to be of acceptable accuracy and provides invaluable information on the rotor flow characteristics. This is evidenced by the good agreement obtained between the predicted results and the available experimental data.

REFERENCES

1. Wu, Chung-Hua, "A General Theory of Three-Dimensional Flow in Subsonic and Supersonic Turbomachines of Axial, Radial and Mixed-Flow Types," National Advisory Committee for Aeronautics, Technical Note TN 2604, 1952.

2. March, H., "A Digital Computer Program for the Through-Flow Fluid Mechanics in an Arbitrary Turbomachine, Using a Matrix Method," A.R.C. R&M No. 3509, 1968.

3. Novak, R.A., "Streamline Curvature Procedures," Journal of Engineering for Power, Ser. A, Vol. 89, No. 4, Oct. 1967, pp. 478-490.

4. Katsanis, T., "Use of Arbitrary Quasi-Orthogonals for Calculating Flow Distribution on a Blade-to-Blade Surface in a Turbomachine," NASA TN D-2546, Dec. 1964.

5. Katsanis, T., "Fortran Program for Calculating Transonic Velocities on a Blade-to-Blade Stream Surface of a Turbomachine," NASA TN D-5427, 1969.

6. Wennerstrom, A.J. and Frost, G.R., "Design of a Rotor Incorporating Splitter Vanes for a High Pressure Ratio Supersonic Axial Compressor Stage," Wright-Patterson AFB, Ohio, ARL TR 74-0110, AD 786025, Aug. 1974.

7. Dring, R.P., "A Momentum Integral Analysis of the Three-Dimensional Turbine End-Wall Boundary Layer," ASME Paper No. 76-GT-6, 1976.

8. Kenny, D.P., "A Method for Calculating Cascade/Channel End Wall Boundary Layer Cross Flow," ASME Paper No. 76-GT-77, 1976.

9. Briley, W.R., "Numerical Method for Predicting Three-Dimensional Steady Viscous Flow in Ducts," Journal of Computational Physics, Vol. 14, 1974, pp. 8-28.

10. Pratap, V.S., Majumda, "Numerical Computation of Flow in Rotating Duct," ASME Paper No. 76-FE-25, 1976.

11. Dodge, P.R., "A Numerical Method for 2-D and 3-D Viscous Flow," AIAA Paper No. 76-425, 1976.

12. Thompson, J.F., Thames, F.C. and Wayne, C., "Automatic Numerical Generation of Body-Fitted Curvilinear Coordinate System for Field Containing Any Number of Arbitrary Two-Dimensional Bodies," Journal of Computational Physics, Vol. 15, 1974, pp. 299-319.

13. Roache, P.J., Computational Fluid Dynamics, Hermosa Publishers, Albuquerque, New Mexico, 1972.

14. Shepherd, D.G., "Principles of Turbomachinery," The Macmillan Company, New York, 1956.

15. Peyret, R. and Viviand, H., "Computation of Viscous Compressible Flows Based on the Navier-Stokes Equations," AGARD AG-212, 1975.

16. Stanitz, J.D., "Two-Dimensional Compressible Flow in Turbomachines with Conic Flow Surfaces," NACA TR 935, 1949.

17. Chu, W.H., "Development of a General Finite Difference Approximation for a General Domain, I. Machine Transformation," J. Comp. Phys., Vol. 8, 1971, p. 932.

18. Amsden, A.A., and Hirst, C.W., "A Simple Scheme for Generating General Curvilinear Grids," J. Comp. Phys., Vol. 11, 1973, p. 348.

19. Godunov, S.K. and Prokopov, G.P., "The Use of Moving Meshes in Gas-Dynamical Computations," USSR Comp. Math. Phys., Vol. 12, 1972, p. 182.

20. Watanabe, I., Ariga, I. and Fujie, K., "A Study of the Flow Patterns through an Impeller Channel of a Radial Turbine," Bulletin of JSME, Vol. 8, No. 30, 1965, pp. 194-200.

21. Benson, R.S., Cartwright, W.G. and Hill, M., "Analytical and Experimental Studies of Two Dimensional Flows in a Radial Bladed Impeller," ASME Paper 71-GT-20, 1971.

22. Gosman, A.D. et al., "Heat and Mass Transfer in Recirculating Flows," Academic Press, London, 1969.

NOMENCLATURE

A_1, A_2, A_5	Coefficients of the finite difference equations.
B_1, B_2, B_5	Coefficients of the finite difference equations.
b	Normal stream annulus thickness, m.
C_1, C_2, C_5	Coefficients of the finite difference equations.
$\bar{C}_1, \bar{C}_2, C_D$	Constants in the turbulence model.
C_p	Specific heat at constant pressure, J/(Kg)(°K).
D	Dissipation function.
$\bar{e}_m$	Unit vector in m-direction.
$\bar{e}_\phi$	Unit vector in ϕ-direction.
$(\bar{e}_n)_\zeta$	Unit vector normal to a constant ζ-line.
$(\bar{e}_n)_\eta$	Unit vector normal to a constant η-line.
$(\bar{e}_t)_\zeta$	Unit vector tangent to a constant ζ-line.
$(\bar{e}_t)_\eta$	Unit vector tangent to a constant η-line.
E	Kinetic energy of turbulence, J/Kg.
G_1, G_2, G_3, G_4, G_5	Donoting source terms in the flow governing equations.
h	Static enthalpy, J/Kg.
h_1, h_2, h_3	Scale factor for the orthogonal curvilinear coordinates.
H	Total enthalpy, J/Kg.
J	Jacobian matrix, E. (B.2).
ℓ	Mixing length, m.
m	Meridional distance, m.
$\dot{M}$	Mass flow per blade flowing through the stream annulus, Kg/sec.
$\bar{n}$	Outward unit normal to the stream surface, S_1, see Fig. 2.

$\bar{N}$	Outward unit normal to blade surface.
N_1, N_2	Components of $\bar{N}$ in m, ϕ directions respectively.
ΔN	Distance of the near-wall grid point (w+1) from the blade surface, see Fig. 5.
p	Static pressure, N/m^2 or blade pitch.
Pr	Effective turbulent Prandtl number.
Pr_ℓ	Molecular Prandtl number.
r	Radius from axis of rotation, m.
R	Universal gas constant, U/(Kg)(°K).
Re	Reynolds number.
S_{CE}	Schmidt number for kinetic energy of turbulence.
$S_{C\varepsilon}$	Schmidt number for dissipation of kinetic energy of turbulence.
t	Time.
T	Temperature, °K.
$\bar{V}$	Absolute velocity vector, m/sec.
V	Magnitude of $\bar{V}$, m/sec.
$\bar{W}$	Relative velocity vector, m/sec.
W	Magnitude of $\bar{W}$, m/sec.
W_1, W_2, W_3	Components of $\bar{W}$ in x_1, x_2 and x_3 directions, respectively.
W_m	Meridional component of the relative velocity vector, m/sec.
W_ϕ	Tangential component of the relative velocity vector, m/sec.
x	Stretched meridional coordinate, Eq. (26).
x_1, x_2, x_3	General orthogonal curvilinear coordinate.

z	Axial coordinate, m.
Z	Number of blades.
α	Angle between m and z, rad., see Fig. 2.
β	Coordinate transformation parameter, Eq. (29), or angle between relative velocity vector and meridional plane, rad., see Fig. 2.
γ	Coordinate transformation parameter, Eq. (29).
δ	Coordinate transformation parameter, Eq. (29).
ρ	Fluid density, Kg/m^3.
τ	Coordinate transformation parameter, Eq. (32b).
σ	Coordinate transformation parameter, Eq. (32b).
μ	Kinematic viscosity, m^2/sec.
μ_e	Effective viscosity, m^2/sec.
μ_ℓ	Laminar viscosity, m^2/sec.
Ω	Rotational speed, rad/sec.
θ	Denotes general flow property and includes ψ, ω, and H.
ϕ	Relative angular coordinate, rad., see Fig. 2.
ψ	Stream function.
ω	Vorticity, 1/sec.
ε	Dissipation of Kinetic energy of turbulence, J/Kg.
ξ	Boundary fitted coordinate, see Fig. 6.
η	Boundary fitted coordinate, see Fig. 6.
Δt	Time step counter.

Superscripts

$-$	Mean value
$*$	Denotes nondimensional quantity.
n	Iteration counter.

Subscripts

e	Effective
ℓ	Laminar.
m	Meridional component.
w	Wall value.
w+1	Pertaining to points in the flow field at a distance $\Delta\eta$ away from w, see Fig. 6.
ϕ	Tangential component.
i,j	Denotes field poistion in (ξ,η) domain, see Fig. 7.
inlet	Inlet or upstream.
exit	Exit or downstream.
total	Total conditions.
tip	Rotor tip.

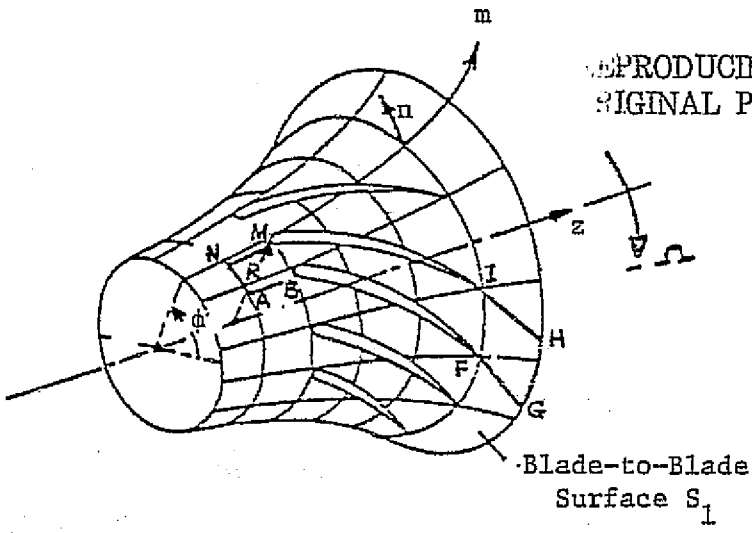

a) BLADE ROW INTERSECTION WITH A STREAM SURFACE.

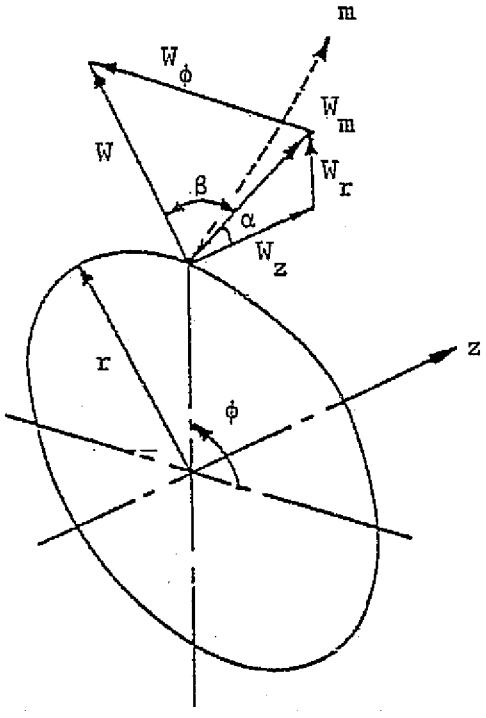

b) COORDINATE SYSTEM AND VELOCITY COMPONENTS.

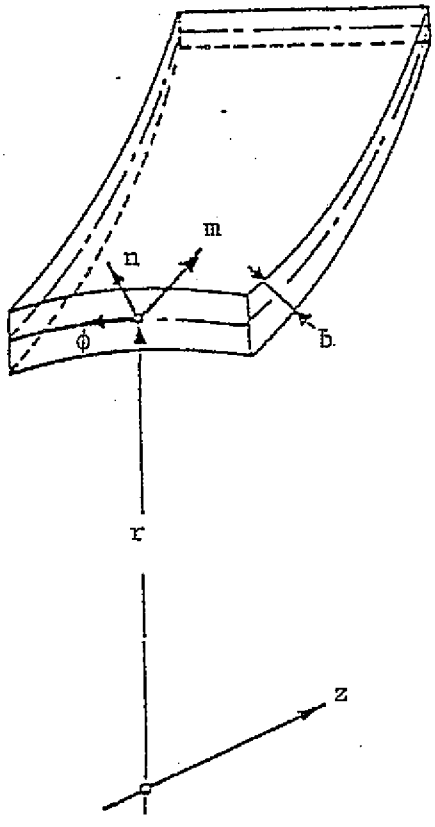

c) DETAILS OF STREAM SURFACE COORDINATE SYSTEM WITH FINITE THICKNESS SHEET.

FIG. 1. BLADE TO BLADE STREAM SURFACE S_1.

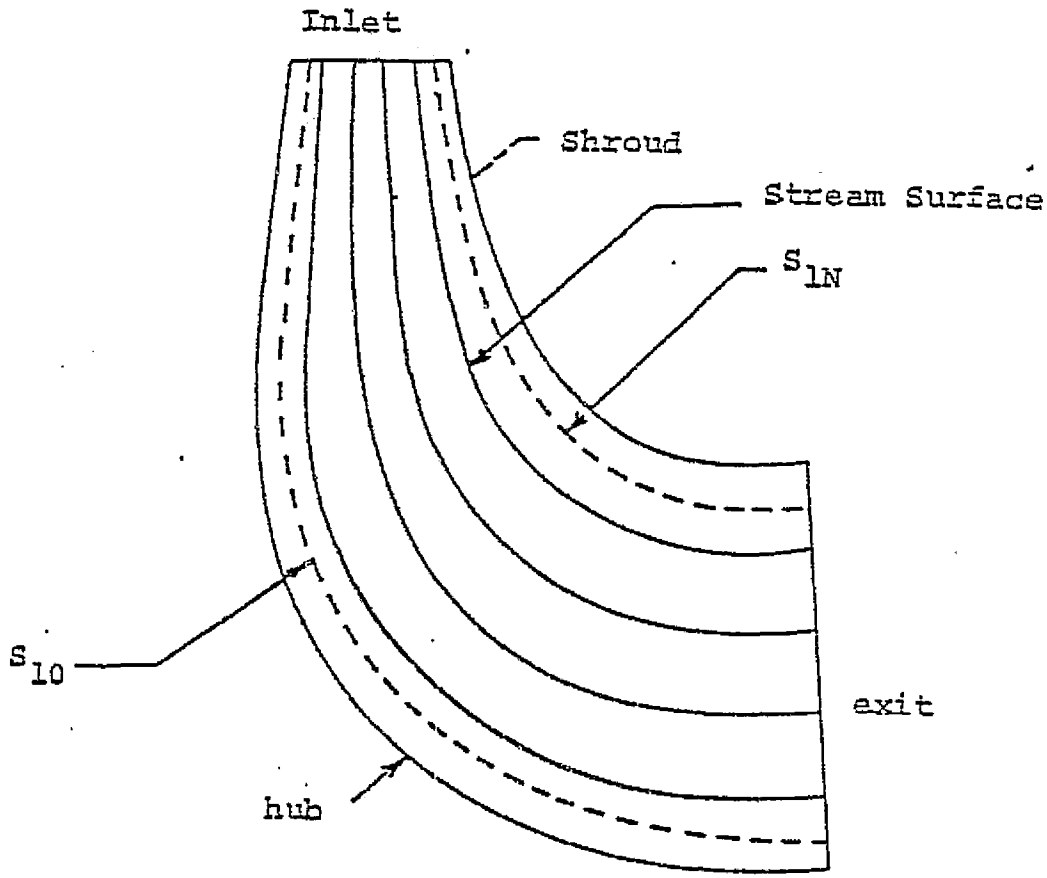

FIG. 2. STREAM SURFACES CONTOURS, OBTAINED FROM A MERIDIONAL FLOW ANALYSIS, FOR A MIXED FLOW MACHINE.

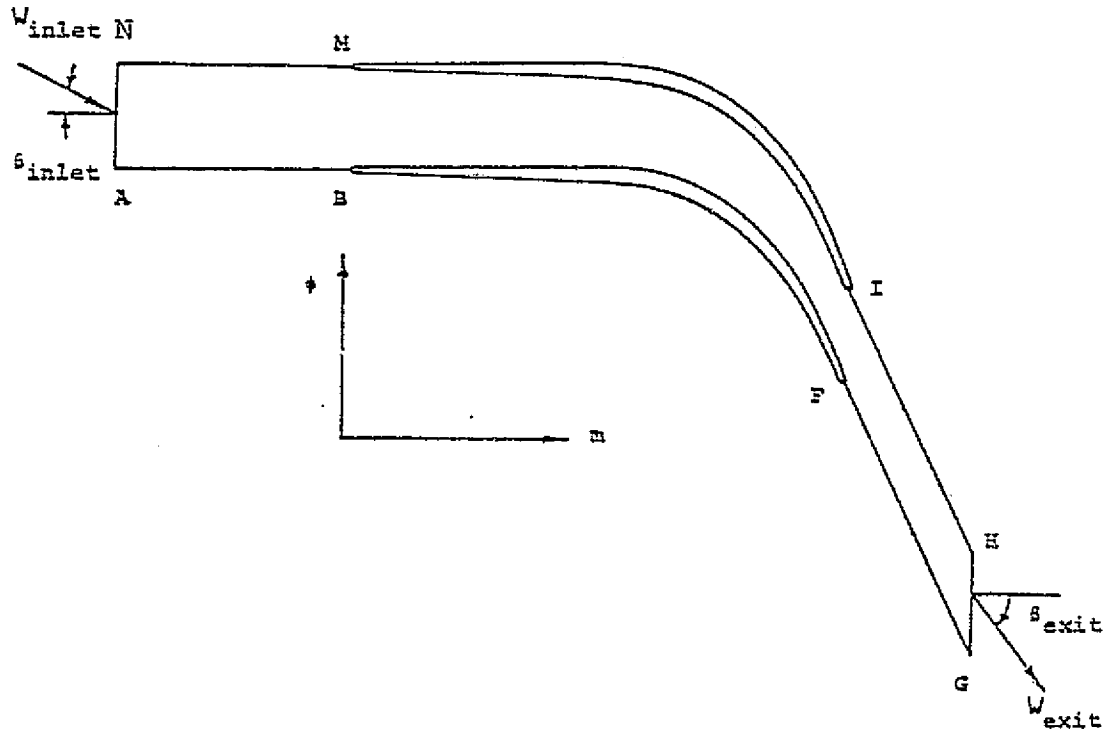

FIG. 3. COMPUTATIONAL DOMAIN IN THE PHYSICAL SPACE.

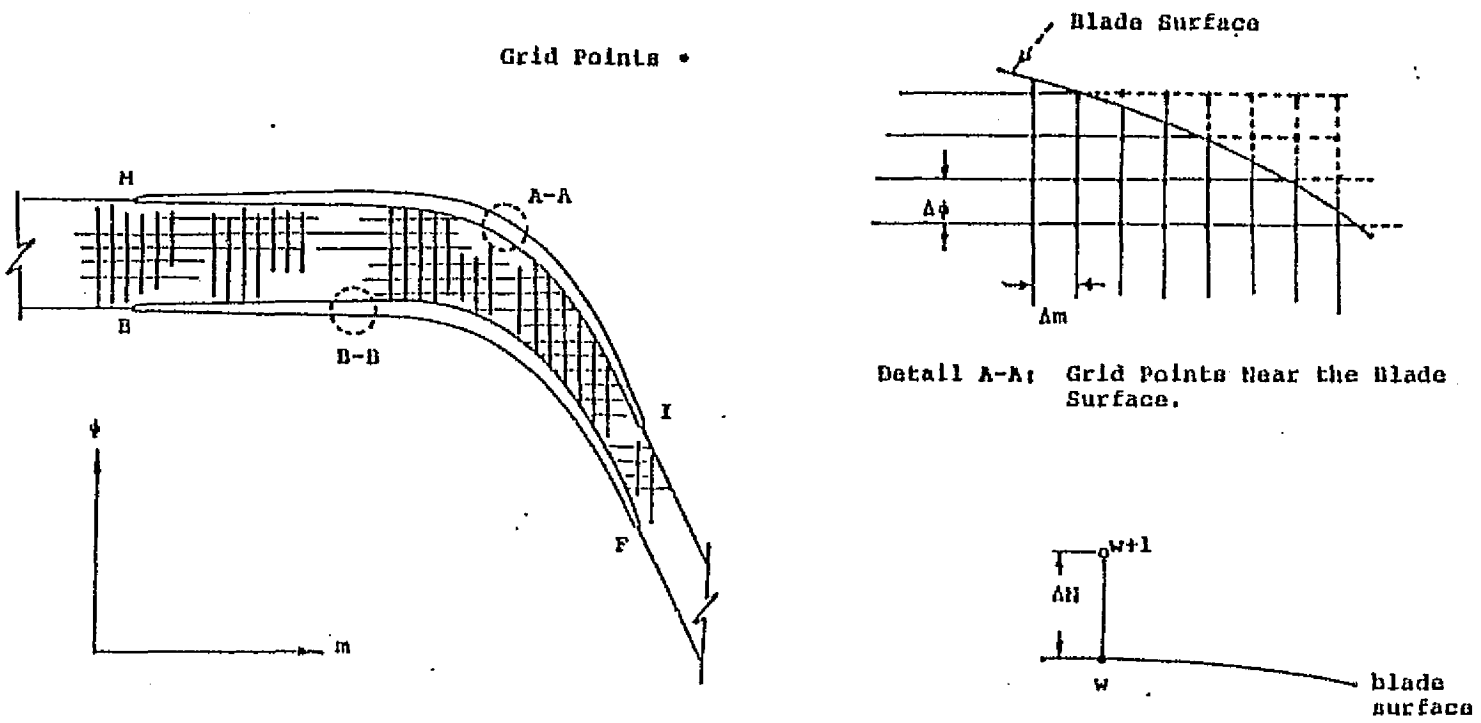

FIG. 4. GRID POINTS NEAR SOLID BOUNDARIES.

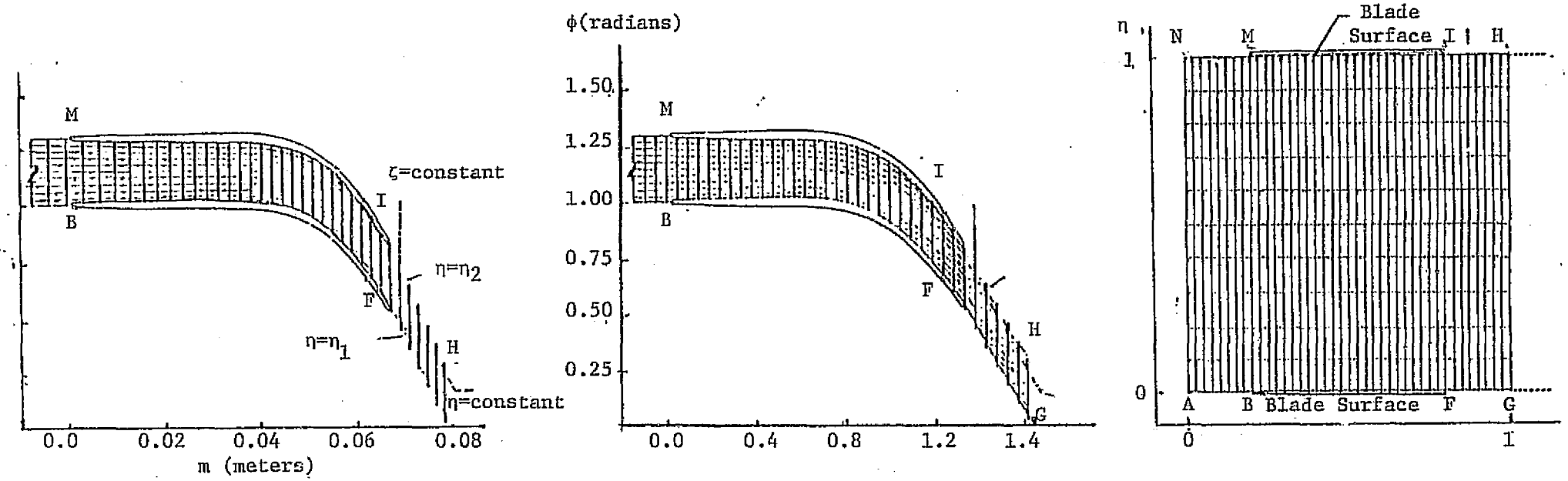

FIG. 5. FIELD TRANSFORMATION.

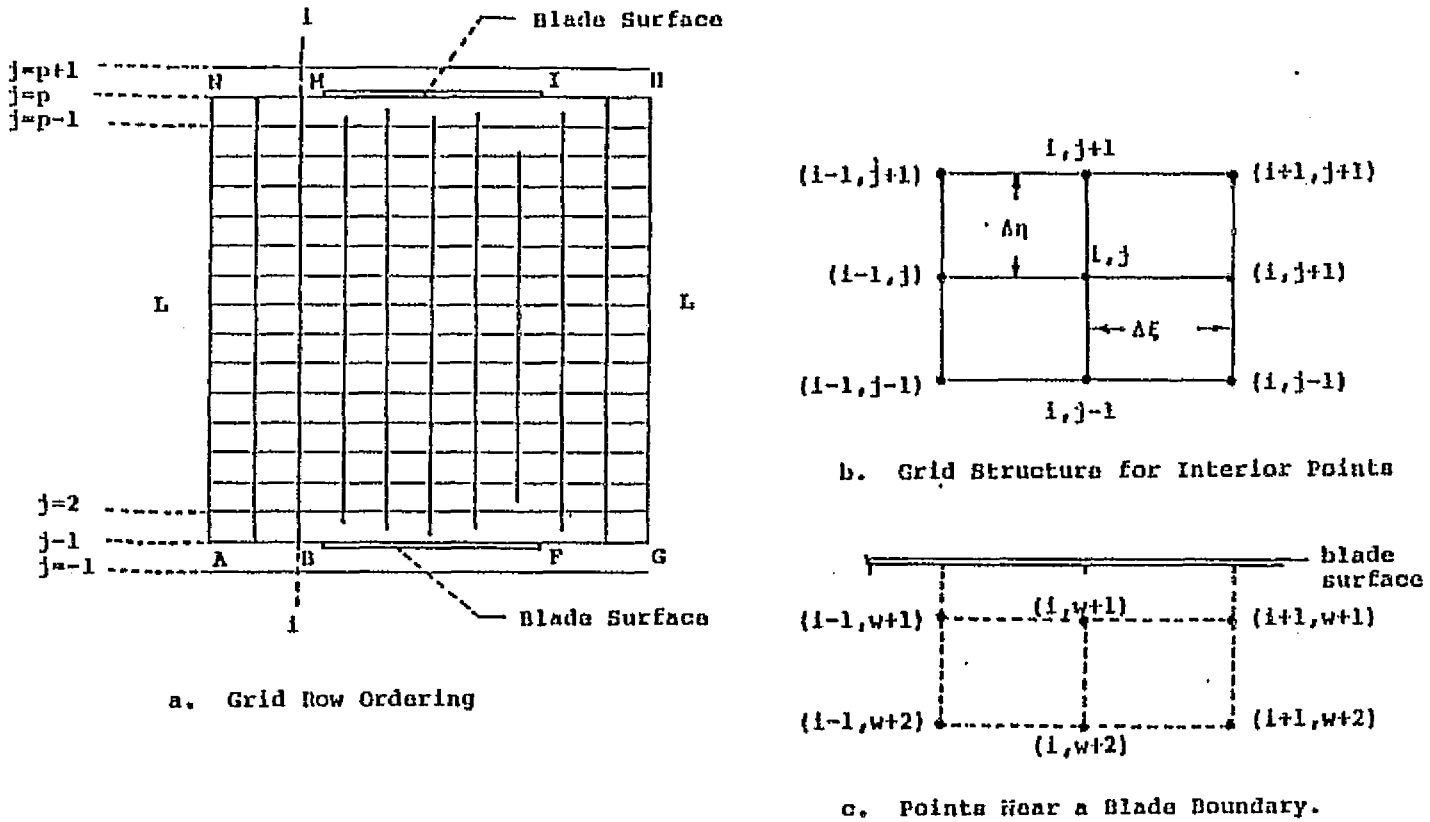

FIG. 6. GRID ORDERING SYSTEM IN THE TRANSFORMED DOMAIN.

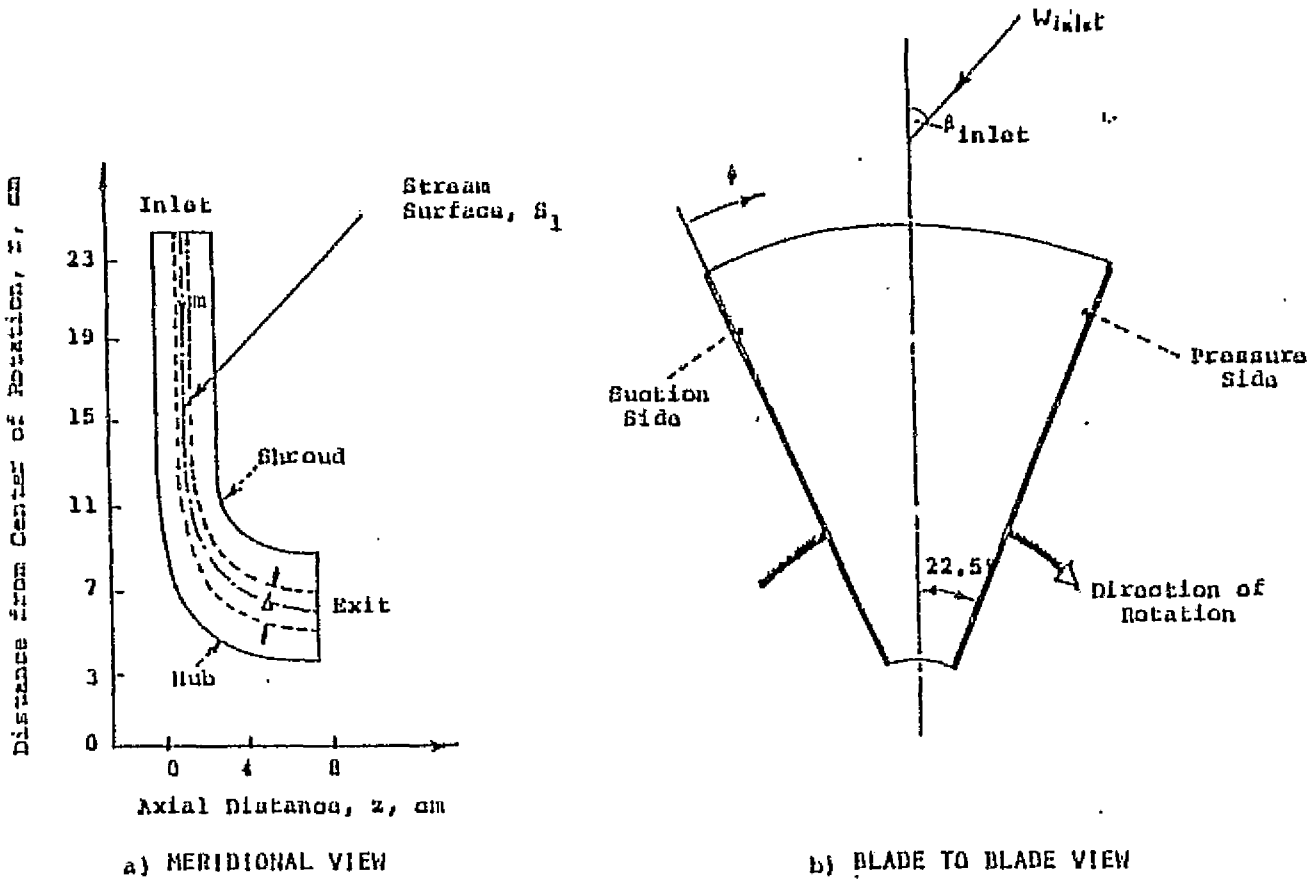

FIG. 7. HUB-SHROUD PROFILE WITH THE STREAM SURFACE S_1, USED FOR BLADE-TO-BLADE ANALYSIS.

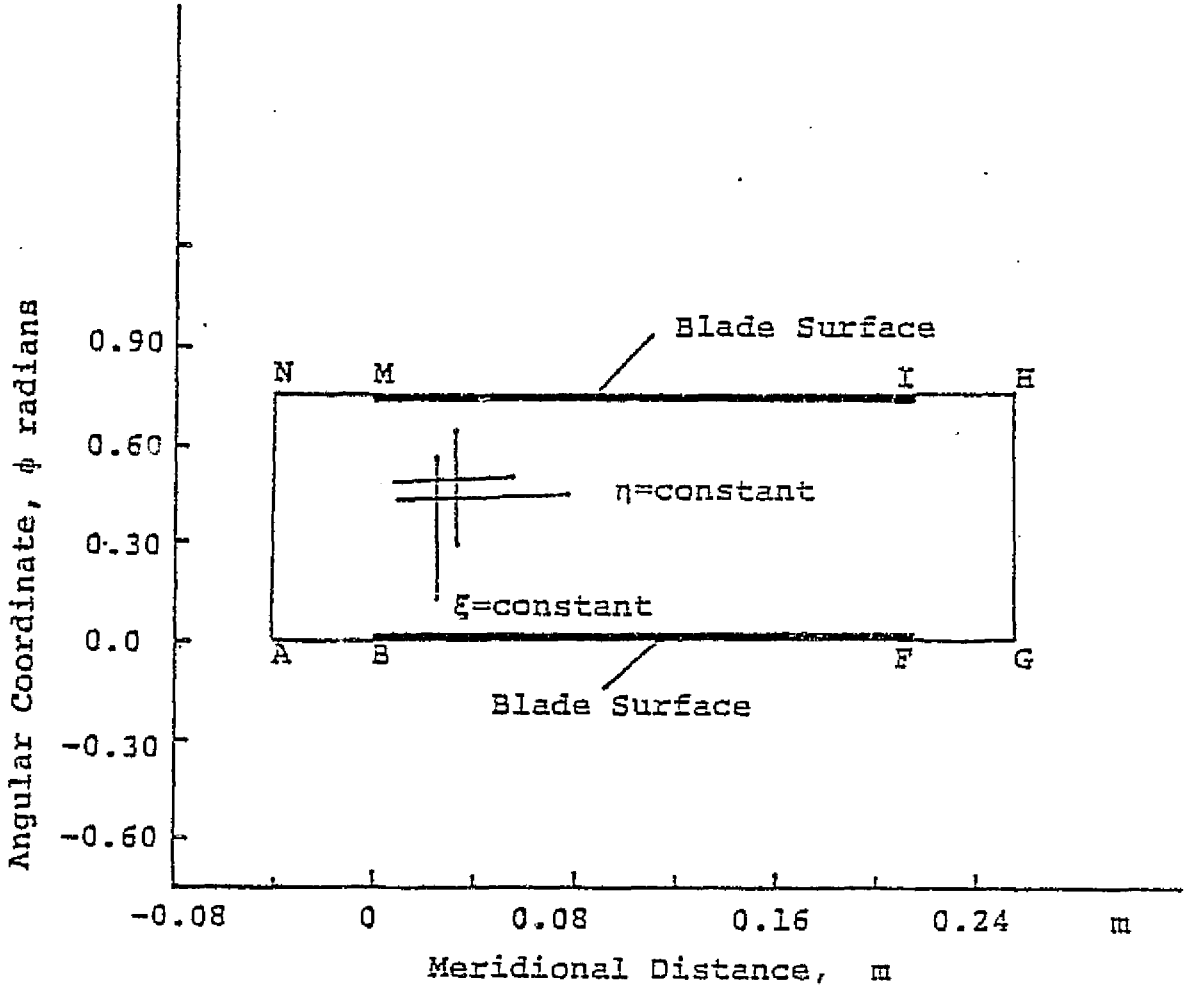

FIG. 8. BLADE-TO-BLADE SHAPE IN THE PHYSICAL DOMAIN FOR THE RADIAL INFLOW TURBINE.

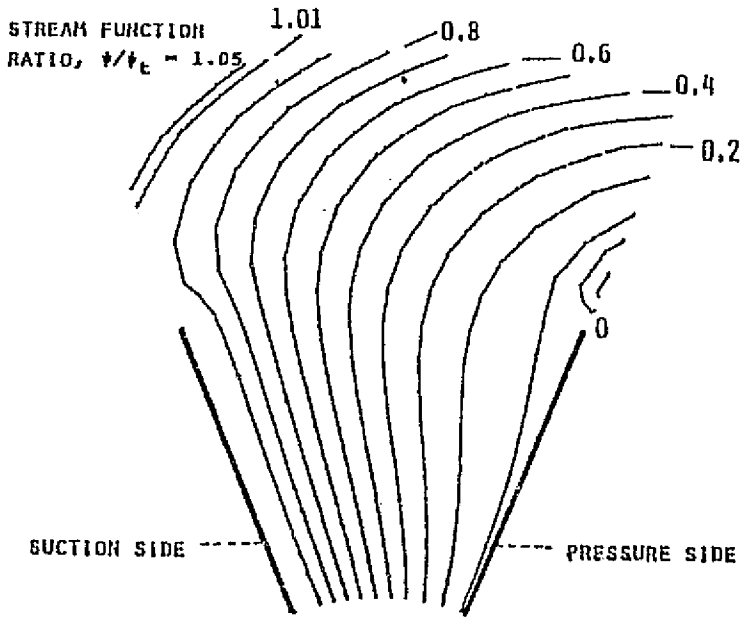

Predicted Case 1

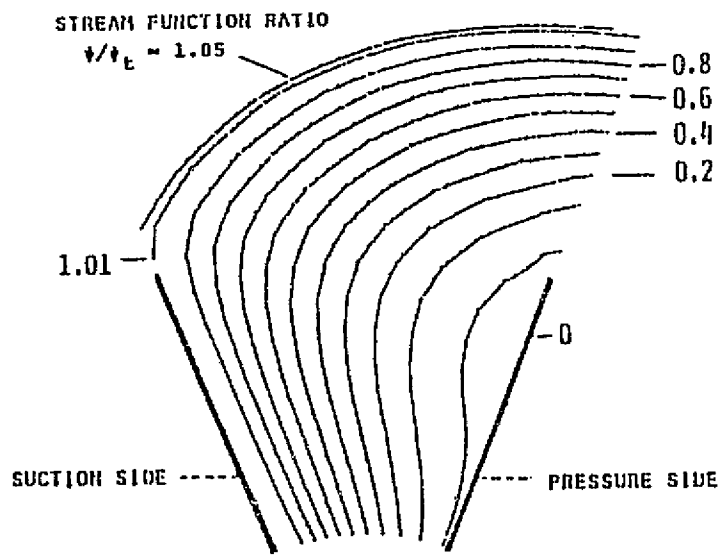

Predicted Case 2

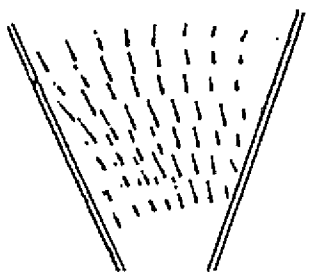

Experimental Case 1

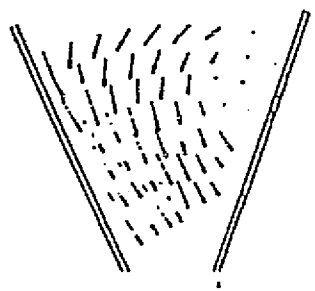

Experimental Case 2

FIG. 9A. RELATIVE STREAMLINES FOR FLOW THROUGH MIXED FLOW TURBINE.

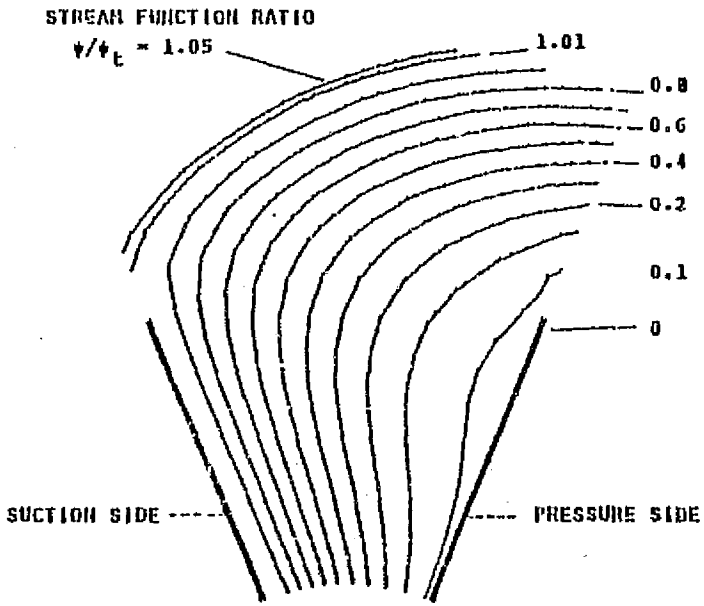

Predicted Case 3

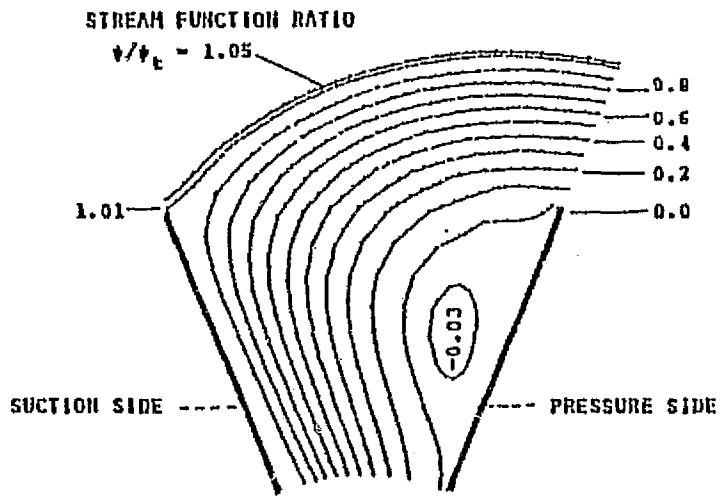

Predicted Case 4

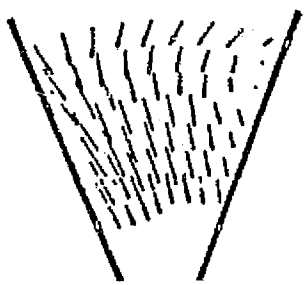

Experimental Case 3

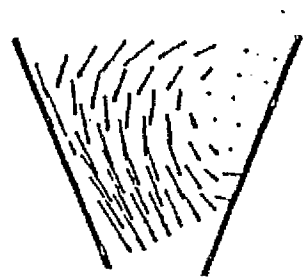

Experimental Case 4

FIG. 9B. RELATIVE STREAMLINES FOR FLOW THROUGH MIXED FLOW TURBINE.

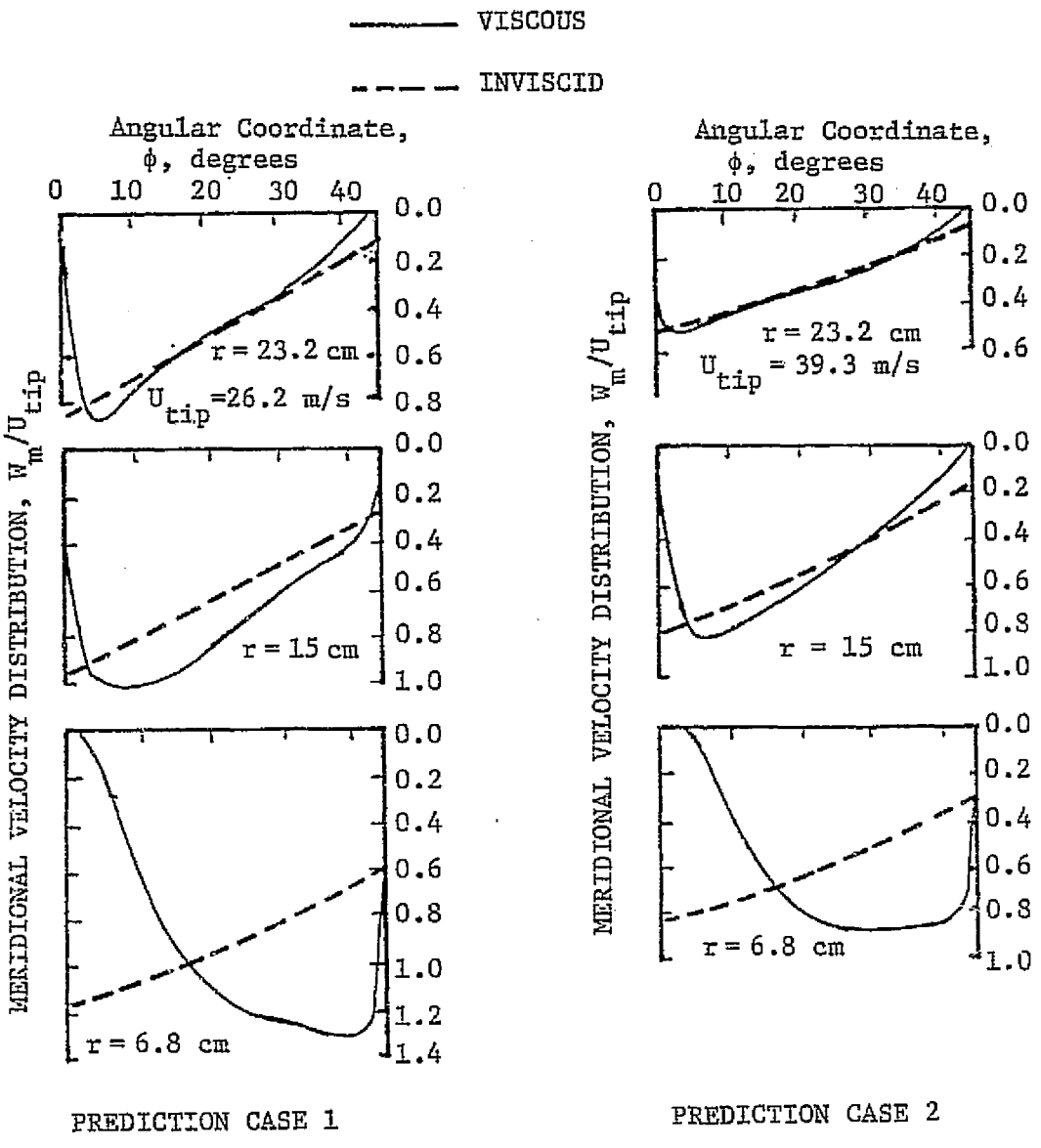

FIG. 10A. NONDIMENSIONAL VELOCITY DISTRIBUTION AT DIFFERENT RADIAL LOCATIONS.

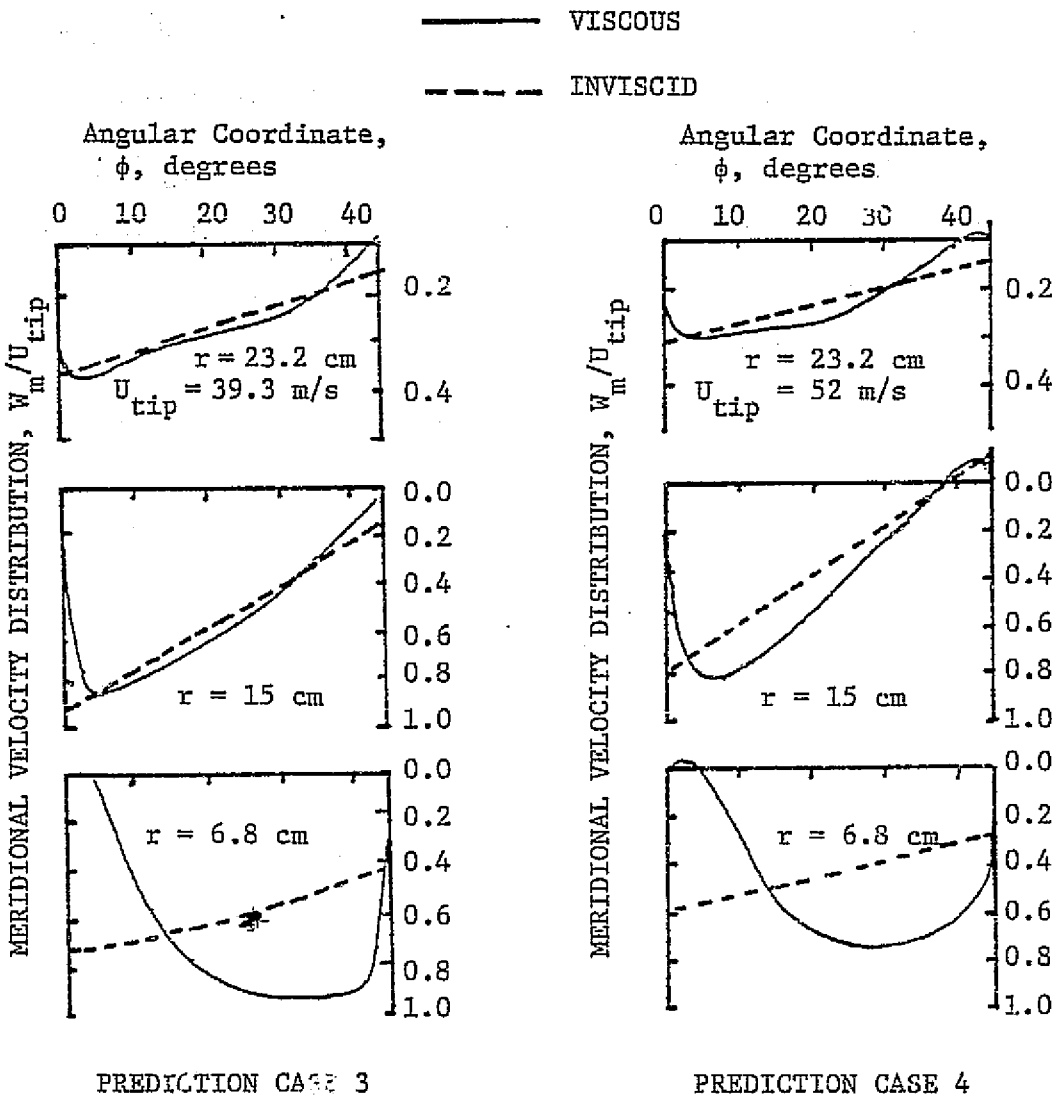

FIG. 10B. NONDIMENSIONAL VELOCITY DISTRIBUTION AT DIFFERENT RADIAL LOCATIONS.

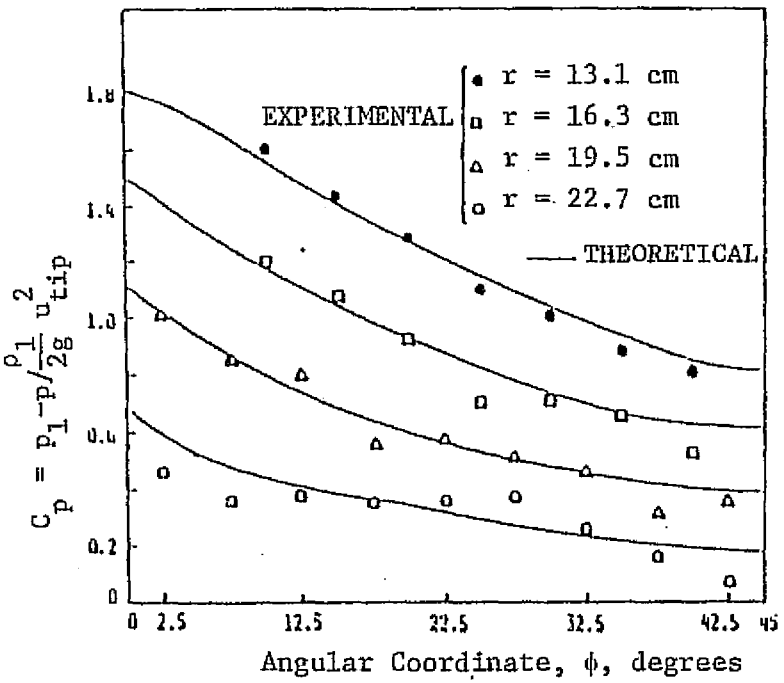

EXPERIMENTAL CASE 1

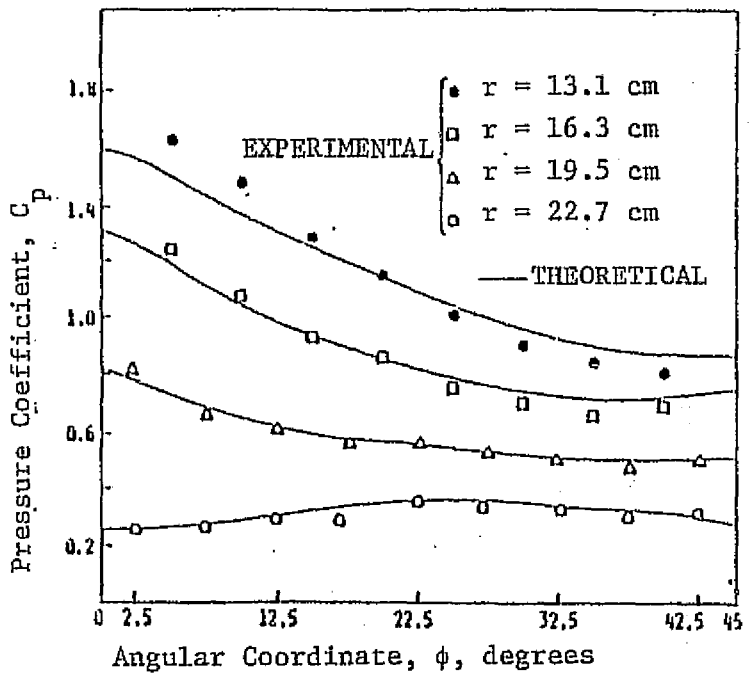

EXPERIMENTAL CASE 2

FIG. 11A. COMPARISON OF PREDICTED STATIC PRESSURE DISTRIBUTION WITH EXPERIMENTAL DATA OF REFERENCE (21).

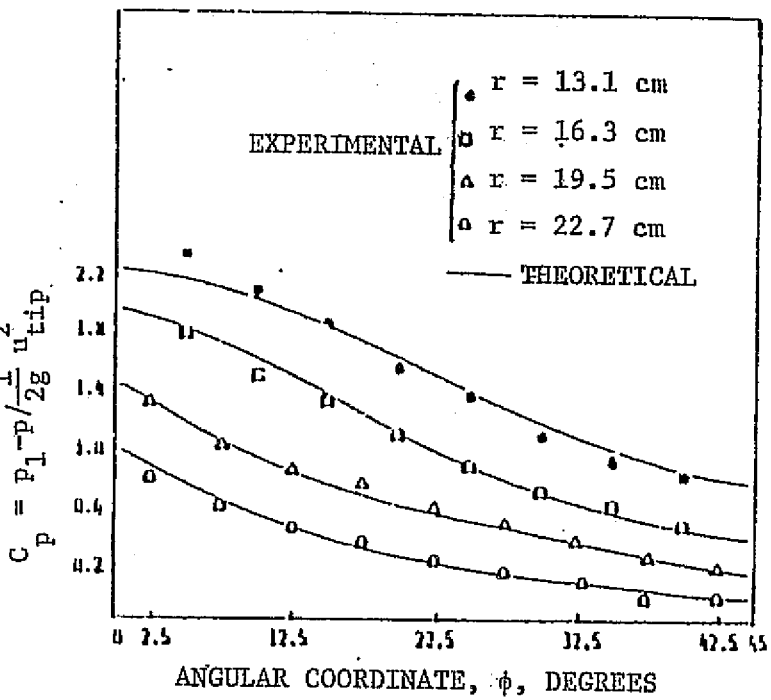

CASE 3

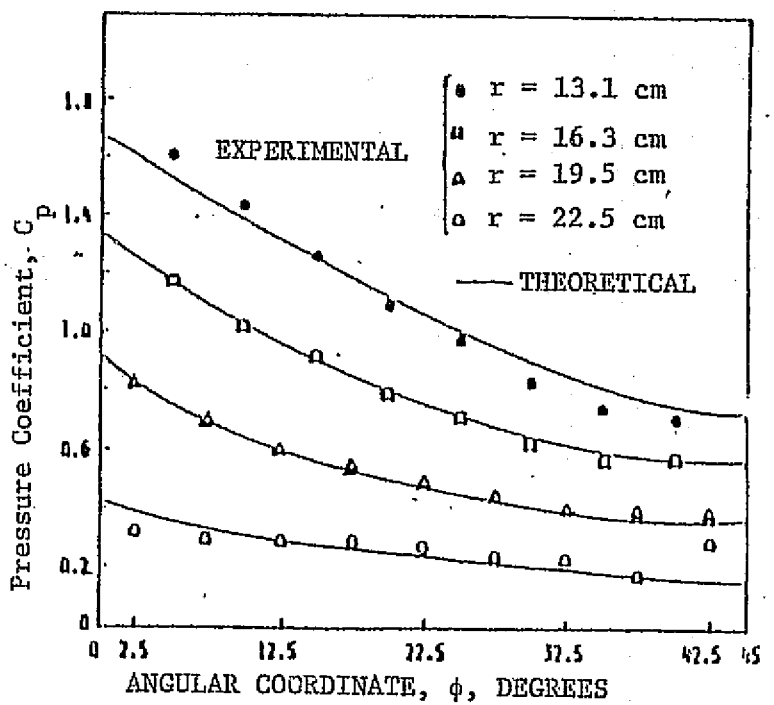

CASE 4

FIG. 11B. COMPARISON OF PREDICTED STATIC PRESSURE DISTRIBUTION WITH EXPERIMENTAL DATA OF REFERENCE (21).

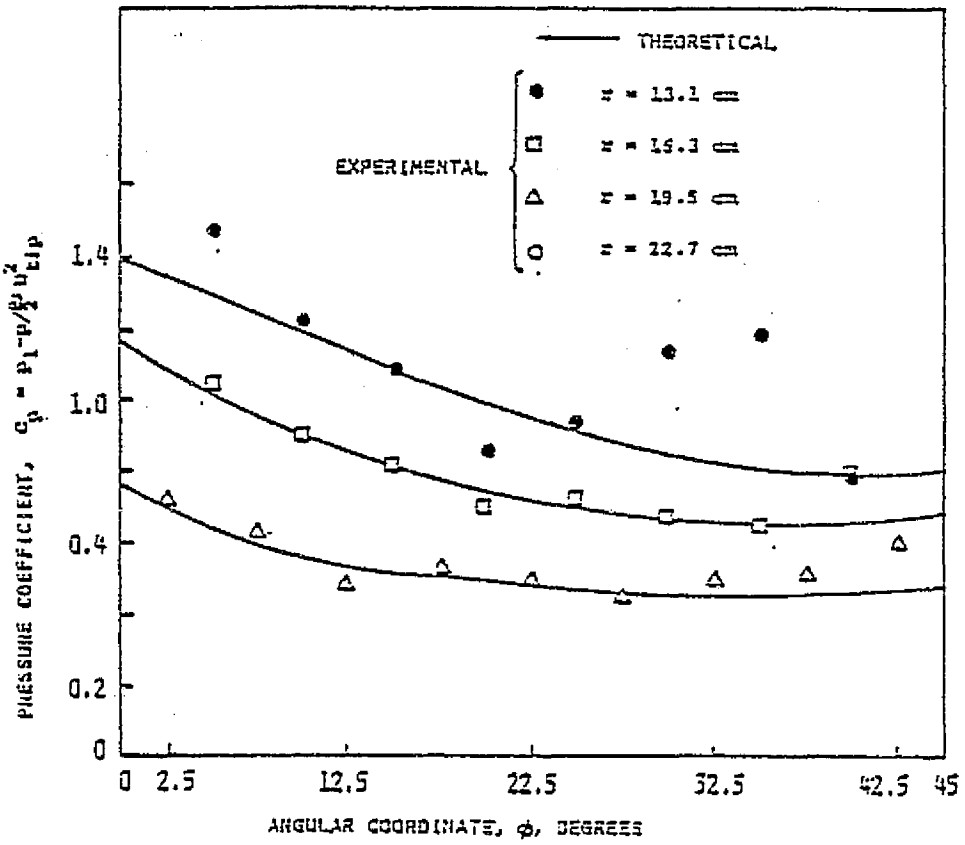

CASE 5

FIG. 11c. COMPARISON OF PREDICTED STATIC PRESSURE DISTRIBUTION WITH EXPERIMENTAL DATA OF REFERENCE (21).

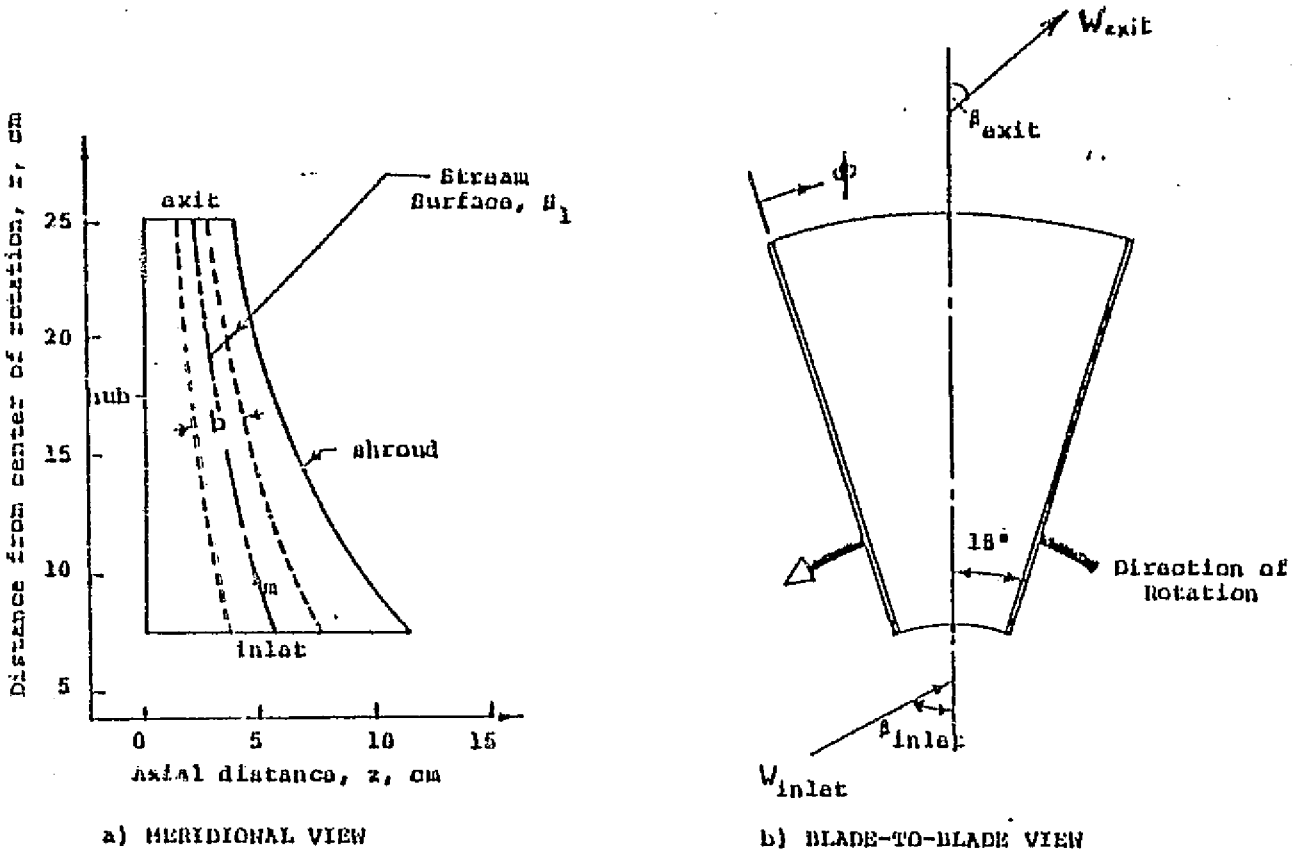

FIG. 12. HUB-SHROUD PROFILE WITH THE STREAM SURFACE, S_1, USED FOR BLADE-TO-BLADE ANALYSIS (COMPRESSOR CASE).

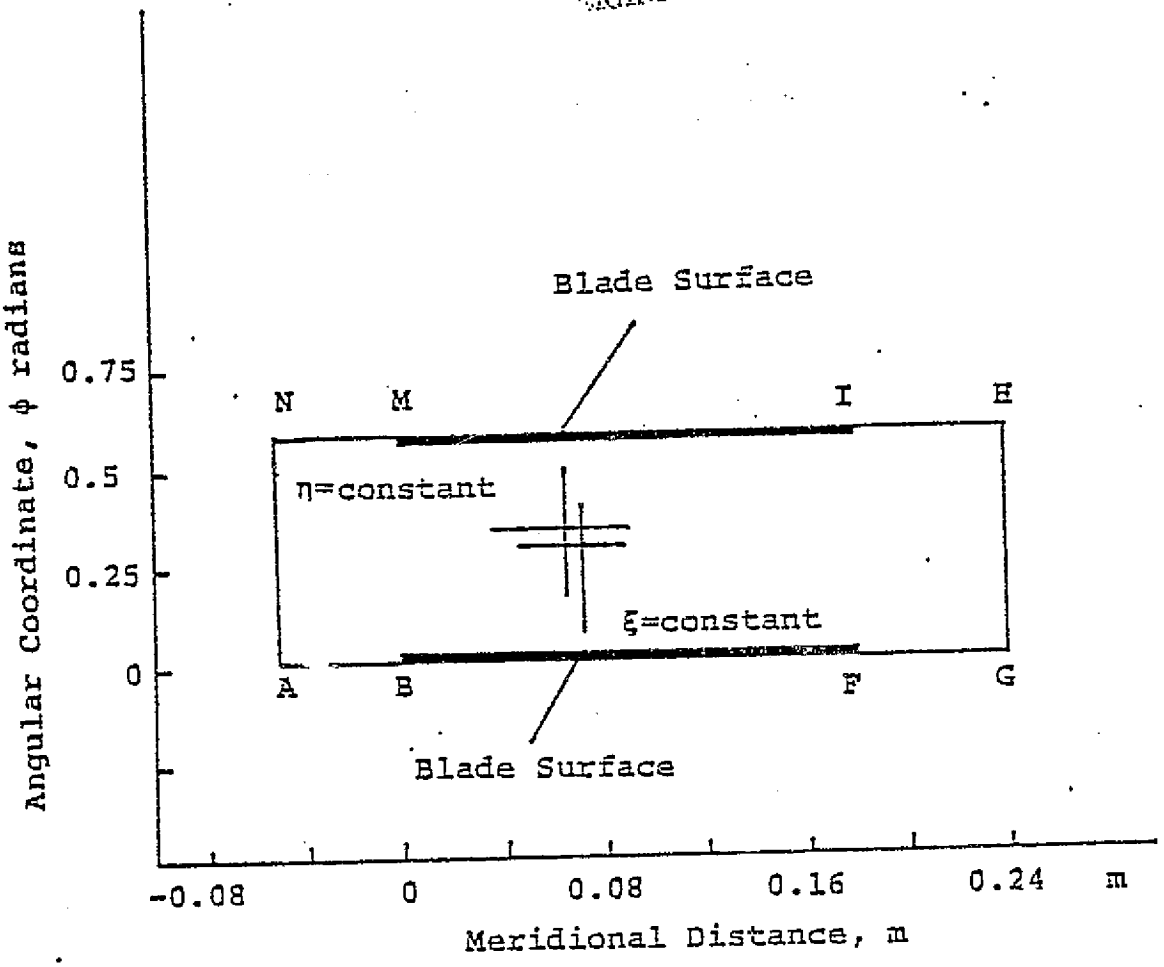

FIG. 13. BLADE-TO-BLADE SHAPE IN THE PHYSICAL DOMAIN FOR THE RADIAL COMPRESSOR.

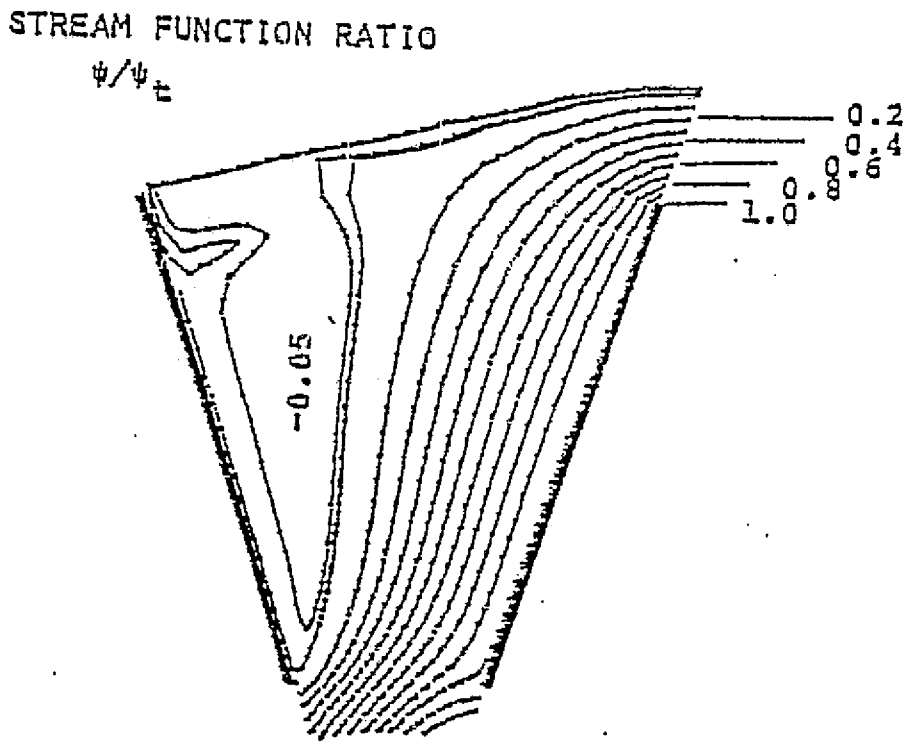

PREDICTED

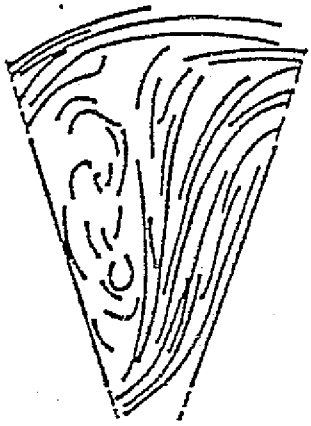

EXPERIMENTAL

FIG. 14. RELATIVE STREAMLINES FOR FLOW THROUGH RADIAL COMPRESSOR.

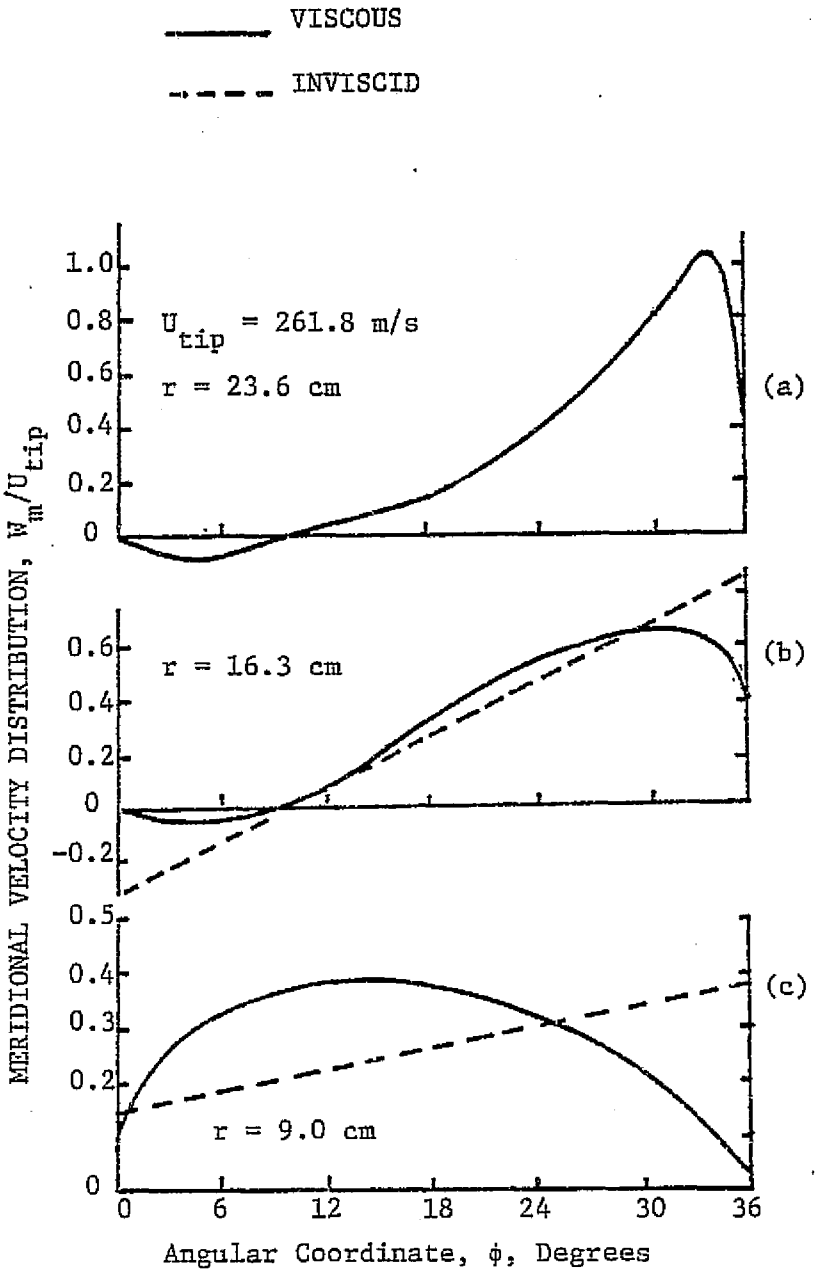

FIG. 10. VELOCITY PROFILES ACROSS THE COMPRESSOR PASSAGES AT DIFFERENT RADIAL LOCATIONS (CASE 5 IN TABLE I).

APPENDIX A

DERIVATION OF STREAM SURFACE EQUATIONS

The detailed derivation of the equations governing the fluid flow on the blade-to-blade computational surface, S_1, of Fig. 2 is presented in this appendix. The complete equations of motion that describe the flow behavior in a turbomachine passage, are first written for a general orthogonal curvilinear coordinate system. A transformation of the resulting equations to the computational coordinates system is then outlined.

Principle Equations in Orthogonal Curvilinear Coordinate

For a general orthogonal curvilinear coordinate system (x_1, x_2, x_3) with scale factors h_1, h_2, h_3, the Navier Stokes equations given as equations (1) and (2) in Section 1 may be written in the following form:

Conservation of Mass:

$$\frac{\partial \rho}{\partial t} + \frac{1}{h_1}\frac{\partial}{\partial x_1}(\rho W_1) + \frac{1}{h_2}\frac{\partial(\rho W_2)}{\partial x_2} + \frac{1}{h_3}\frac{\partial}{\partial x_3}(\rho W_3)$$

$$+ \frac{\rho W_1}{h_1}\left(\frac{1}{h_2}\frac{\partial h_2}{\partial x_1} + \frac{1}{h_3}\frac{\partial h_3}{\partial x_1}\right) + \frac{\rho W_2}{h_2}\left(\frac{1}{h_1}\frac{\partial h_1}{\partial x_2} + \frac{1}{h_3}\frac{\partial h_3}{\partial x_2}\right)$$

$$+ \frac{\rho W_3}{h_3}\left(\frac{1}{h_1}\frac{\partial h_1}{\partial x_3} + \frac{1}{h_2}\frac{\partial h_2}{\partial x_3}\right) = 0 \qquad \text{(A.1)}$$

where W_1, W_2, W_3 are the components of the velocity vector $\vec{W}$ in the x_1, x_2 and x_3 directions respectively.

Conservation of Momentum in x_1 Direction

$$\rho\left[\frac{\partial W_1}{\partial t} + \frac{W_1}{h_1}\frac{\partial W_1}{\partial x_1} + \frac{W_2}{h_2}\frac{\partial W_1}{\partial x_2} + \frac{W_3}{h_3}\frac{\partial W_1}{\partial x_3} - \frac{W_2}{h_1}\left(\frac{W_2}{h_2}\frac{\partial h_2}{\partial x_1} - \frac{W_1}{h_2}\frac{\partial h_1}{\partial x_2}\right)\right.$$

$$\left. + \frac{W_3}{h_1}\left(\frac{W_1}{h_3}\frac{\partial h_1}{\partial x_3} - \frac{W_3}{h_3}\frac{\partial h_3}{\partial x_1}\right) + 2(\Omega_2 W_3 - \Omega_3 W_2) - \frac{\Omega^2}{2}\frac{1}{h_1}\frac{\partial r^2}{\partial x_1}\right]$$

$$= -\frac{1}{h_1}\frac{\partial p}{\partial x_1} - \frac{2}{3}\frac{1}{h_1}\frac{\partial}{\partial x_1}(\mu_e \nabla\cdot\vec{W})$$

$$+ \frac{1}{h_1 h_2 h_3}\left\{\frac{\partial}{\partial x_1}\left[2\mu_e h_2 h_3\left(\frac{1}{h_1}\frac{\partial W_1}{\partial x_1} + \frac{W_2}{h_1 h_2}\frac{\partial h_1}{\partial x_2} + \frac{W_3}{h_3 h_1}\frac{\partial h_1}{\partial x_3}\right)\right]\right.$$

$$+ \frac{\partial}{\partial x_2}\left[\mu_e h_1 h_3\left(\frac{h_2}{h_1}\frac{\partial}{\partial x_1}\left(\frac{W_2}{h_2}\right) + \frac{h_1}{h_2}\frac{\partial}{\partial x_2}\left(\frac{W_1}{h_1}\right)\right)\right]$$

$$\left. + \frac{\partial}{\partial x_3}\left[\mu_e h_1 h_2\left(\frac{h_1}{h_3}\frac{\partial}{\partial x_3}\left(\frac{W_1}{h_1}\right) + \frac{h_3}{h_1}\frac{\partial}{\partial x_1}\left(\frac{W_3}{h_3}\right)\right)\right]\right\}$$

$$+ \frac{\mu_e}{h_1 h_2}\left\{\frac{h_2}{h_1}\frac{\partial}{\partial x_1}\left(\frac{W_2}{h_2}\right) + \frac{h_1}{h_2}\frac{\partial}{\partial x_2}\left(\frac{W_1}{h_1}\right)\right\}\cdot\frac{\partial h_1}{\partial x_2}$$

$$+ \frac{\mu_e}{h_1 h_3}\left\{\frac{h_1}{h_3}\frac{\partial}{\partial x_3}\left(\frac{W_1}{h_1}\right) + \frac{h_3}{h_1}\frac{\partial}{\partial x_1}\left(\frac{W_3}{h_3}\right)\right\}\cdot\frac{\partial h_1}{\partial x_3}$$

$$- \frac{2\mu_e}{h_1 h_2}\left\{\frac{1}{h_2}\frac{\partial W_2}{\partial x_2} + \frac{W_3}{h_2 h_3}\frac{\partial h_2}{\partial x_3} + \frac{W_1}{h_1 h_2}\frac{\partial h_2}{\partial x_1}\right\}\cdot\frac{\partial h_2}{\partial x_1}$$

$$- \frac{2\mu_e}{h_1 h_3}\left\{\frac{1}{h_3}\frac{\partial W_3}{\partial x_3} + \frac{W_1}{h_3 h_1}\frac{\partial h_3}{\partial x_1} + \frac{W_3}{h_2 h_3}\frac{\partial h_3}{\partial x_2}\right\}\cdot\frac{\partial h_3}{\partial x_1} \qquad \text{(A.2)}$$

where

$$\nabla\cdot\vec{W} = \frac{1}{h_1}\frac{\partial W_1}{\partial x_1} + \frac{1}{h_2}\frac{\partial W_2}{\partial x_2} + \frac{1}{h_3}\frac{\partial W_3}{\partial x_3} + \frac{W_1}{h_1}\left(\frac{1}{h_2}\frac{\partial h_2}{\partial x_1} + \frac{1}{h_3}\frac{\partial h_3}{\partial x_1}\right)$$

$$+ \frac{W_2}{h_2}\left(\frac{1}{h_1}\frac{\partial h_1}{\partial x_2} + \frac{1}{h_3}\frac{\partial h_3}{\partial x_2}\right) + \frac{W_3}{h_3}\left(\frac{1}{h_1}\frac{\partial h_1}{\partial x_3} + \frac{1}{h_2}\frac{\partial h_2}{\partial x_3}\right) \qquad \text{(A.2a)}$$

Conservation of Momentum in x_2 Direction:

$$\rho\left[\frac{\partial W_2}{\partial t} + \frac{W_1}{h_1}\frac{\partial W_2}{\partial x_1} + \frac{W_2}{h_2}\frac{\partial W_2}{\partial x_2} + \frac{W_3}{h_3}\frac{\partial W_2}{\partial x_3} - \frac{W_3}{h_2}\left(\frac{W_3}{h_3}\frac{\partial h_3}{\partial x_2} - \frac{W_2}{h_3}\frac{\partial h_2}{\partial x_3}\right)\right.$$

$$\left. + \frac{W_1}{h_2}\left(\frac{W_2}{h_1}\frac{\partial h_2}{\partial x_1} - \frac{W_1}{h_1}\frac{\partial h_1}{\partial x_2}\right) + 2(\Omega_3 W_1 - \Omega_1 W_3) - \frac{\Omega^2}{2h_2}\frac{\partial r^2}{\partial x^2}\right]$$

$$= -\frac{1}{h_2}\frac{\partial p}{\partial x_2} - \frac{2}{3}\frac{1}{h_2}\frac{\partial}{\partial x_2}(\mu_e \nabla\cdot\bar{W})$$

$$+ \frac{1}{h_1 h_2 h_3}\left\{\frac{\partial}{\partial x_1}\left[h_2 h_3 \mu_e\left(\frac{h_2}{h_1}\frac{\partial}{\partial x_1}\left(\frac{W_2}{h_2}\right) + \frac{h_1}{h_2}\frac{\partial}{\partial x_2}\left(\frac{W_1}{h_1}\right)\right)\right]\right.$$

$$+ \frac{\partial}{\partial x_2}\left[2\mu_e h_1 h_3\left(\frac{1}{h_2}\frac{\partial W_2}{\partial x_2} + \frac{W_3}{h_2 h_3}\frac{\partial h_2}{\partial x_3} + \frac{W_1}{h_1 h_2}\frac{\partial h_2}{\partial x_1}\right)\right]$$

$$\left. + \frac{\partial}{\partial x_3}\left[\mu_e h_1 h_2\left(\frac{h_3}{h_2}\frac{\partial}{\partial x_2}\left(\frac{W_3}{h_3}\right) + \frac{h_2}{h_3}\frac{\partial}{\partial x_3}\left(\frac{W_2}{h_2}\right)\right)\right]\right\}$$

$$+ \frac{\mu_e}{h_2 h_3}\left[\frac{h_3}{h_2}\frac{\partial}{\partial x_2}\left(\frac{W_3}{h_3}\right) + \frac{h_2}{h_3}\frac{\partial}{\partial x_3}\left(\frac{W_2}{h_2}\right)\right]\cdot\frac{\partial h_2}{\partial x_3}$$

$$+ \frac{\mu_e}{h_2 h_1}\left[\frac{h_2}{h_1}\frac{\partial}{\partial x_1}\left(\frac{W_2}{h_2}\right) + \frac{h_1}{h_2}\frac{\partial}{\partial x_2}\left(\frac{W_1}{h_1}\right)\right]\cdot\frac{\partial h_2}{\partial x_1}$$

$$- \frac{2\mu_e}{h_2 h_3}\left[\frac{1}{h_3}\frac{\partial W_3}{\partial x_3} + \frac{W_1}{h_3 h_1}\frac{\partial h_3}{\partial x_1} + \frac{W_2}{h_2 h_3}\frac{\partial h_3}{\partial x_2}\right]\cdot\frac{\partial h_3}{\partial x_2}$$

$$- \frac{2\mu_e}{h_2 h_1}\left[\frac{1}{h_1}\frac{\partial W_1}{\partial x_1} + \frac{W_2}{h_1 h_2}\frac{\partial h_1}{\partial x_2} + \frac{W_3}{h_3 h_1}\frac{\partial h_1}{\partial x_3}\right]\cdot\frac{\partial h_1}{\partial x_2} \qquad (A.3)$$

Conservation of Momentum in x_3 Direction:

$$\rho\left[\frac{\partial W_3}{\partial t} + \frac{W_1}{h_1}\frac{\partial W_3}{\partial x_1} + \frac{W_2}{h_2}\frac{\partial W_3}{\partial x_2} + \frac{W_3}{h_3}\frac{\partial W_3}{\partial x_3} - \frac{W_1}{h_3}\left(\frac{W_1}{h_1}\frac{\partial h_1}{\partial x_3} - \frac{W_3}{h_1}\frac{\partial h_3}{\partial x_1}\right)\right.$$

$$\left. + \frac{W_2}{h_3}\left(\frac{W_3}{h_2}\frac{\partial h_3}{\partial x_2} - \frac{W_2}{h_2}\frac{\partial h_2}{\partial x_3}\right) + 2(\Omega_1 W_2 - \Omega_2 W_1) - \frac{\Omega^2}{2}\frac{1}{h_3}\frac{\partial r^2}{\partial x_3}\right]$$

$$= -\frac{1}{h_3}\frac{\partial p}{\partial x_3} - \frac{2}{3}\frac{1}{h_3}\frac{\partial}{\partial x_3}\left(\mu_e \nabla\cdot\bar{W}\right)$$

$$+ \frac{1}{h_1 h_2 h_3}\left\{\frac{\partial}{\partial x_1}\left[h_2 h_3 \mu_e\left(\frac{h_1}{h_3}\frac{\partial}{\partial x_3}\left(\frac{W_1}{h_1}\right) + \frac{h_3}{h_1}\frac{\partial}{\partial x_1}\left(\frac{W_3}{h_3}\right)\right)\right]\right.$$

$$+ \frac{\partial}{\partial x_2}\left[h_1 h_3 \mu_e\left(\frac{h_3}{h_2}\frac{\partial}{\partial x_2}\left(\frac{W_3}{h_3}\right) + \frac{h_2}{h_3}\frac{\partial}{\partial x_3}\left(\frac{W_2}{h_2}\right)\right)\right]$$

$$\left. + \frac{\partial}{\partial x_3}\left[2h_1 h_2 \mu_e\left(\frac{1}{h_3}\frac{\partial W_3}{\partial x_3} + \frac{W_1}{h_3 h_1}\frac{\partial h_3}{\partial x_1} + \frac{W_2}{h_2 h_3}\frac{\partial h_3}{\partial x_2}\right)\right]\right\}$$

$$+ \frac{\mu_e}{h_1 h_3}\left[\frac{h_1}{h_3}\frac{\partial}{\partial x_3}\left(\frac{W_1}{h_1}\right) + \frac{h_3}{h_1}\frac{\partial}{\partial x_1}\left(\frac{W_3}{h_3}\right)\right]\cdot\frac{\partial h_3}{\partial x_1}$$

$$+ \frac{\mu_e}{h_2 h_3}\left[\frac{h_3}{h_2}\frac{\partial}{\partial x_2}\left(\frac{W_3}{h_3}\right) + \frac{h_2}{h_3}\frac{\partial}{\partial x_3}\left(\frac{W_2}{h_2}\right)\right]\cdot\frac{\partial h_3}{\partial x_2}$$

$$- \frac{2\mu_e}{h_1 h_3}\left[\frac{1}{h_1}\frac{\partial W_1}{\partial x_1} + \frac{W_2}{h_1 h_2}\frac{\partial h_1}{\partial x_2} + \frac{W_3}{h_3 h_1}\frac{\partial h_1}{\partial x_3}\right]\cdot\frac{\partial h_1}{\partial x_3}$$

$$- \frac{2\mu_e}{h_2 h_3}\left[\frac{1}{h_2}\frac{\partial W_2}{\partial x_2} + \frac{W_3}{h_2 h_3}\frac{\partial h_2}{\partial x_3} + \frac{W_1}{h_1 h_2}\frac{\partial h_2}{\partial x_1}\right]\cdot\frac{\partial h_2}{\partial x_3} \qquad (A.4)$$

In the above equations Ω_1, Ω_2, Ω_3 are the components of the rotor angular velocity, $\bar{\Omega}$, in the x_1, x_2, x_3 directions respectively.

Flow Equations on Blade-to-Blade Computational Surface S_1:

Starting from equations (A.1), (A.2) and (A.3), the flow equations over a blade-to-blade computational surface is formulated. In deriving the required equations, one has to describe the computational surface S_1 in terms of the orthogonal curvilinear coordinates x_1, x_2 and x_3,

$$S_1(x_1, x_2, x_3) = 0 \tag{A.5}$$

Equation (A.5) is used to relate any flow property q of the three dimensional flow field with the same flow property $\bar{q}$ on the surface S_1. In general

$$\bar{q} = q(x_1, x_2, x_3) \tag{A.6}$$

Since x_3 on the surface S_1 is not an independent variable, therefore,

$$\bar{q} = q[x_1, x_2, x_3(x_1, x_2)] = q(x_1, x_2) \tag{A.7}$$

The relation between the partial derivatives of the flow property q in the three-dimensional field with those on the surface S_1 can be written as:

$$\frac{\partial \bar{q}}{\partial x_1} = \frac{\partial q}{\partial x_1} - \frac{n_1}{n_3}\frac{h_1}{h_3}\frac{\partial q}{\partial x_3}$$

$$\frac{\partial \bar{q}}{\partial x_2} = \frac{\partial q}{\partial x_2} - \frac{n_2}{n_3}\frac{h_2}{h_3}\frac{\partial q}{\partial x_3} \tag{A.8}$$

where n_1, n_2, and n_3 are the components of a unit vector $\bar{n}$ that is normal to the prescribed surface in the x_1, x_2 and x_3 directions, respectively.

The previous derivation is valid for any generalized curvilinear coordinate system. Following Wu [1], the best coordinate choice for the surface S_1 are the meridional distance m, the tangential angle ϕ and the normal distance n to the surface (see Fig. 1).

The following relations apply for the (m-ϕ-n) coordinate system

$$n_1 = n_2 = 0 \ , \qquad n_3 = 1 \tag{A.9}$$

and the metric or Lamie coefficients h_1, h_2, h_3 are given by:

$$h_1 = 1 \ , \quad h_2 = r \ , \quad h_3 = 1 \tag{A.10}$$

In the present study, the number of the surfaces, to which the passage is divided, is chosen to be large. Therefore, the filament thickness b or each surface is considered to be small compared to the radius r. Consequently, for those surfaces which are located away from the hub and shroud boundaries (Fig. 3), one can consider that the change of flow properties across the filament thickness, b, is neglected. Thus

$$\frac{\partial q}{\partial x_3} = \frac{\partial q}{\partial n_3} = 0 \tag{A.11}$$

Using equations (A.9), (A.10) and (A.11) to rewrite the right hand side of equation (A.9), we obtain

$$\frac{\partial \bar{q}}{\partial x_1} = \frac{\partial q}{\partial x_1} = \frac{\partial q}{\partial m} \tag{A.12}$$

$$\frac{\partial \bar{q}}{\partial x_2} = \frac{\partial q}{\partial x_2} = \frac{\partial q}{\partial \phi} \tag{A.13}$$

Substituting the expressions in equations (A.11), (A.12) and (A.13) for the derivatives of all quantities in the equations of motion (A.1), (A.2) and (A.3), we obtain:

Conservation of Mass

$$\frac{\partial \rho}{\partial t} + \frac{\partial}{\partial m}(\rho W_m) + \frac{1}{r}\frac{\partial}{\partial \phi}(\rho W_\phi) + \frac{\rho}{r} W_m \frac{\partial r}{\partial m} = 0 \qquad \text{(A.14)}$$

where W_m and W_ϕ are the components of relative velocity vector in the meridional and tangential direction respectively.

Conservation of Momentum in the Meridional Direction

$$\rho \frac{\partial W_m}{\partial t} + \rho\left(W_m \frac{\partial W_m}{\partial m} + \frac{W_\phi}{r}\frac{\partial W_m}{\partial \phi} - \frac{W^2_\phi}{r}\sin\alpha - \Omega^2 r \sin\alpha - 2\Omega W_\phi \sin\alpha\right)$$

$$= -\frac{\partial p}{\partial m} - \frac{2}{3}\frac{\partial}{\partial m}\left[\mu_e\left(\frac{\partial W_m}{\partial m} + \frac{W_m}{r}\sin\alpha + \frac{1}{r}\frac{\partial W_\phi}{\partial \phi}\right)\right]$$

$$+ \frac{1}{r}\left\{\frac{\partial}{\partial m}\left(2\mu_e r \frac{\partial W_m}{\partial m}\right) + \frac{\partial}{\partial \phi}\left[\mu_e\left(\frac{\partial W_\phi}{\partial m} - \frac{W_\phi}{r}\sin\alpha + \frac{1}{r}\frac{\partial W_m}{\partial \phi}\right)\right]\right.$$

$$\left. - 2\frac{\mu_e}{r}\left[\frac{1}{r}\frac{\partial W_\phi}{\partial \phi} + \frac{W_m}{r}\sin\alpha\right]\sin\alpha\right\} \qquad \text{(A.15)}$$

where α is the angle between the meridional streamline and the axis of rotation (z), as shown in Fig. 1, such that $\sin\alpha = \frac{dr}{dm}$.

Conservation of Momentum in the Tangential Direction

$$\rho r \frac{\partial W_\phi}{\partial t} + \rho\left(r W_m \frac{\partial W_\phi}{\partial m} + W_\phi \frac{\partial W_\phi}{\partial \phi} + W_m W_\phi \sin\alpha + 2\Omega r W_m \sin\alpha\right)$$

$$= -\frac{\partial p}{\partial \phi} - \frac{2}{3}\frac{\partial}{\partial \phi}\left[\mu_e\left(\frac{\partial W_m}{\partial m} + \frac{W_m}{r}\sin\alpha + \frac{1}{r}\frac{\partial W_\phi}{\partial \phi}\right)\right]$$

$$+ \frac{\partial}{\partial m}\left[\mu_e\left(r\frac{\partial W_\phi}{\partial m} - W_\phi \sin\alpha + \frac{\partial W_m}{\partial \phi}\right)\right] + \frac{\partial}{\partial \phi}\left[2\mu_e\left(\frac{1}{r}\frac{\partial W_\phi}{\partial \phi} + \frac{W_m}{r}\sin\alpha\right)\right]$$

$$+ \mu_e \sin\alpha\left[\frac{\partial W_\phi}{\partial m} - \frac{W_\phi}{r}\sin\alpha + \frac{1}{r}\frac{\partial}{\partial \phi} W_m\right] \qquad \text{(A.16)}$$

Adopting equations (A.14), (A.15) and (A.16) leads to a system that contains derivatives with respect to two space variables only, namely m and ϕ. Consequently, the flow over the surface S_1 may be treated in a two dimensional manner.

In order to obtain an equation for a stream function, reference [1] introduces the concept of an integrating factor, b, such that the equation of continuity becomes:

$$br \frac{\partial \rho}{\partial t} + \frac{\partial}{\partial m} (br \rho W_m) + \frac{\partial}{\partial \phi} (b \rho W_\phi) = 0 \qquad (A.17)$$

where the factor, b, satisfies the following relation,

$$\frac{W_m}{b} \frac{\partial b}{\partial m} + \frac{W_\phi}{br} \frac{\partial}{\partial \phi} b = 0 \qquad (A.18)$$

A stream function may now be defined such that

$$W_m = \frac{\dot{M}}{b} \frac{1}{\rho r} \frac{\partial \psi}{\partial \phi} \quad , \quad W_\phi = - \frac{\dot{M}}{b} \frac{1}{\rho} \frac{\partial \psi}{\partial m} \qquad (A.19)$$

The previous equations indicate that the integrating factor, b, is nothing more than the filament thickness of the surface S_1.

It is worth noting that the above system of equations are valid for any computational surface providing that its geometry has been defined. The system can be applied in the rotating frame as stated, or in the absolute stationary frame by setting $\Omega = 0$. When $\frac{dr}{dm} = 1$ or $\alpha = 90°$, the equations represent the flow in a pure radial machine. Also, when $\frac{dr}{dm} = 0$ or $\alpha = 0°$, the equations represent the flow in an axial machine.

Energy Equation

For steady relative flow through a turbomachine rotor, the conservation of energy given as equation (3) in Section 1, can be rewritten in the following form:

$$\rho\bar{W}\cdot\nabla h = \bar{W}\cdot\nabla p + D + \nabla\cdot(\frac{\mu_e}{Pr}\nabla h) \tag{A.20}$$

where Pr is the Prandtl number and D is the energy dissipation function.

It is more convenient to express the energy equation (A.20) in terms of the total enthalpy H of the gas, and its velocity components. The total enthalpy for turbulent flow is expressed as follows.

$$H = h + W^2/2 + \Omega W_\phi r + \Omega^2 r^2/2 + E \tag{A.21}$$

where E is the kinetic energy of turbulence.

Using the above equation, the energy equation (A.20) reduces to:

$$\rho\bar{W}\cdot\nabla H = \rho\bar{W}\cdot\nabla[\frac{W^2}{2} + \Omega W_\phi r + \frac{\Omega^2 r^2}{2} + E] + \bar{W}\cdot\nabla p + \nabla\cdot[\frac{\mu_e}{Pr}\nabla(H - \frac{W^2}{2} - \Omega W_\phi r - \frac{\Omega^2 r^2}{2} - E)] + D \tag{A.22}$$

Equation (A.22) may be expressed in a slightly different form by eliminating the pressure term in the right hand side using the momentum equation (1) of Section 1, with the following result

$$\rho\bar{W}\cdot\nabla H = \rho\bar{W}\cdot\nabla[\Omega W_\phi r + \Omega^2 r^2 + E] + \nabla\cdot[\frac{\mu_e}{Pr}\nabla(H - \frac{W^2}{2} - \Omega W_\phi r - \frac{\Omega^2 r^2}{2} - E)] - \bar{W}\cdot\nabla(\mu_e\bar{\omega}) + \frac{4}{3}\bar{W}\cdot\nabla(\mu_e\nabla\cdot\bar{W}) + D \tag{A.23}$$

It is to be noted that in formulating the above relation, use has been made of the following vector identities:

$$\bar{W}\cdot\bar{\Omega}\times\bar{W} = 0 \quad , \quad \bar{W}\cdot\bar{W}\cdot\nabla\,\bar{W} = \bar{W}\cdot\nabla\,\frac{W^2}{2}$$

$$\bar{W}\cdot\bar{R} = \bar{W}\cdot\nabla\,\frac{r^2}{2} \quad , \quad \nabla\times\bar{W} = \bar{\omega}$$

where $\bar{\omega}$ is the vorticity vector.

In order to preserve simplicity of concept and for better organization, it would be very advantageous, as pointed out in ref. [22], to replace the kinetic energy of turbulence convective term, $\rho\bar{W}\cdot\nabla E$, that appear in the above equation by its equivalent diffusion expression. The exact form can be expressed, using the transport equation of the kinetic energy of turbulence, as follows:

$$\rho\bar{W}\cdot\nabla E \equiv \nabla\cdot\left(\frac{\mu_e}{S_{CE}}\nabla E\right) \tag{A.24}$$

where S_{CE} has the significance of Schmidt number for the kinetic energy of turbulence. It is worth noting that the adoption of equation (A.24) implies that the generation and decay terms in the full kinetic energy of turbulence equation are in balance.

Substituting now equation (A.24) in (A.23), we obtain:

$$\rho\bar{W}\cdot\nabla H = \rho\bar{W}\cdot\nabla[\Omega W_\phi r + \Omega^2 r^2] + \nabla\cdot\left[\frac{\mu_e}{Pr}\nabla\left(H - \frac{W^2}{2} - \Omega W_\phi r - \frac{\Omega^2 r^2}{2} - E\right) + \frac{\mu_e}{S_{CE}}\nabla E\right] - \bar{W}\cdot\nabla\times(\mu_e\bar{\omega}) + \frac{4}{3}\bar{W}\cdot\nabla(\mu_e\nabla\cdot\bar{W}) + D \tag{A.25}$$

For the (m,ϕ,n) coordinate system, associated with the computational surface S_1 of Fig. 1, the ∇ operator can be expressed as

$$\nabla = \bar{e}_m \frac{\partial}{\partial m} + \frac{\bar{e}_\phi}{r} \frac{\partial}{\partial \phi} \tag{A.26}$$

where $\bar{e}_m$ and $\bar{e}_\phi$ denote unit vectors in the meridional and tangential directions respectively. The velocity vector $\bar{W}$, and the vorticity vector $\bar{\omega}$, may be written as follows in this system of coordinates:

$$\bar{W} = W_m \bar{e}_m + W_\phi \bar{e}_\phi = \frac{\dot{M}}{b} \frac{1}{\rho} \left[\frac{1}{r} \frac{\partial \psi}{\partial \phi} \bar{e}_m - \frac{\partial \psi}{\partial m} \bar{e}_\phi\right]$$

$$\bar{\omega} = \omega \bar{n} \tag{A.27}$$

When the relations (A.26) and (A.27) are used to fully expand the energy equation (A.25), the following result is obtained.

$$\frac{\dot{M}}{b} \left[\frac{\partial}{\partial m}\left(H \frac{\partial \psi}{\partial \phi}\right) - \frac{\partial}{\partial \phi}\left(H \frac{\partial \psi}{\partial m}\right)\right] - \frac{\partial}{\partial m}\left(\frac{\mu_e}{Pr} r \frac{\partial H}{\partial m}\right) - \frac{1}{r} \frac{\partial}{\partial \phi}\left(\frac{\mu_e}{Pr} \frac{\partial H}{\partial \phi}\right)$$

$$+ \frac{\partial}{\partial m}\left\{\mu_e r \left[\frac{1}{Pr} \frac{\partial W^2/2}{\partial m} - \left(\frac{1}{S_{CE}} - \frac{1}{Pr}\right) \frac{\partial E}{\partial m}\right]\right\}$$

$$+ \frac{\partial}{\partial \phi}\left\{\frac{\mu_e}{r}\left[\frac{1}{Pr} \frac{\partial W^2/2}{\partial \phi} - \left(\frac{1}{S_{CE}} - \frac{1}{Pr}\right) \frac{\partial E}{\partial \phi}\right]\right\} - W_\phi \frac{\partial}{\partial m}\left(\mu_e \omega\right)$$

$$+ \frac{W_m}{r} \frac{\partial}{\partial \phi}\left(\mu_e \omega\right) - Dr + G_2 = 0 \tag{A.28}$$

where

$$G_2 = -\Omega \frac{\dot{M}}{b}\left\{\frac{\partial}{\partial m}\left[\left(W_\phi r + r^2\Omega\right) \frac{\partial \psi}{\partial \phi}\right] - \frac{\partial}{\partial \phi}\left[\left(W_\phi r + r^2\Omega\right) \frac{\partial \psi}{\partial m}\right]\right\}$$

$$+ \Omega\left\{\frac{\partial}{\partial m}\left[\frac{\mu_e}{Pr} r \frac{\partial}{\partial m}\left(W_\phi r + \frac{\Omega r^2}{2}\right)\right] + \frac{1}{r} \frac{\partial}{\partial \phi}\left[\frac{\mu_e}{Pr} \frac{\partial}{\partial \phi}\left(W_\phi r + \frac{\Omega r^2}{2}\right)\right]\right\} \tag{A.29}$$

and the dissipation function, D, is given by

$$D = 2\mu_e \left\{\left(\frac{\partial W_m}{\partial m}\right)^2 + \left(\frac{1}{r}\frac{\partial W_\phi}{\partial \phi} + \frac{W_m}{r}\sin\alpha\right)^2\right\}$$

$$+ \mu_e \left\{\frac{\partial W_\phi}{\partial m} + \frac{1}{r}\frac{\partial W_m}{\partial \phi} - \frac{W_\phi}{r}\sin\alpha\right\}^2 \qquad \text{(A.30)}$$

APPENDIX B

DERIVATIVE TRANSFORMATION

This appendix presents the mathematical expressions used to transform the partial derivatives from the physical space of (m,ϕ) coordinates to the computational domain of (ξ,η) coordinates. A few relations involving directional derivatives either normal or tangent to a line of constant ξ as well as a line of constant η are also included. Since the purpose of this appendix is to provide a quick reference only, most of the algebraic development is omitted.

Partial Derivative Transformation

As pointed out earlier in Section 2, two transformations are employed to transform the physical space of Fig. 5a into the unit square of Fig. 5c. These transformations are given by equations (31) and (35). The partial derivatives of any scalar function, f, are transformed utilizing the chain rule as follows:

$$\frac{\partial f}{\partial m} = \frac{\partial f}{\partial x}\frac{\partial x}{\partial m} + \frac{\partial f}{\partial \phi}\frac{\partial \phi}{\partial m} = \frac{1}{r}\frac{\partial f}{\partial x}$$

$$= \frac{1}{r}\left(\frac{\partial f}{\partial \xi}\frac{\partial \xi}{\partial x} + \frac{\partial f}{\partial \eta}\frac{\partial \eta}{\partial x}\right)$$

$$= \frac{1}{rJ}\left(\frac{\partial \phi}{\partial \eta}\frac{\partial f}{\partial \xi} - \frac{\partial \phi}{\partial \xi}\frac{\partial f}{\partial \eta}\right) \qquad \text{(B.1)}$$

$$\frac{\partial f}{\partial \phi} = \frac{\partial f}{\partial \xi}\frac{\partial \phi}{\partial \xi} + \frac{\partial f}{\partial \eta}\frac{\partial \eta}{\partial \phi}$$

$$= \left(\frac{\partial x}{\partial \xi}\frac{\partial f}{\partial \eta} - \frac{\partial x}{\partial \eta}\frac{\partial f}{\partial \xi}\right)/J \qquad \text{(B.2)}$$

where J is the Jacobian of transformation given by:

$$J = \frac{\partial x}{\partial \xi}\frac{\partial \phi}{\partial \eta} - \frac{\partial x}{\partial \eta}\frac{\partial \phi}{\partial \xi} \tag{B.3}$$

Likewise, higher order derivatives, which appear in the flow governing equations, are transformed using the following relations:

$$\begin{aligned} r\frac{\partial}{\partial m}\left(r\frac{\partial f}{\partial m}\right) &= \frac{\partial^2 f}{\partial x^2} \\ &= \frac{1}{J^2}\left[\left(\frac{\partial \phi}{\partial \eta}\right)^2\frac{\partial^2 f}{\partial \xi^2} - 2\frac{\partial \phi}{\partial \xi}\frac{\partial \phi}{\partial \eta}\frac{\partial^2 f}{\partial \xi \partial \eta} + \left(\frac{\partial \phi}{\partial \xi}\right)^2\frac{\partial^2 f}{\partial \eta^2}\right] \\ &+ \frac{1}{J^3}\left\{\left[\left(\frac{\partial \phi}{\partial \eta}\right)^2\frac{\partial^2 \phi}{\partial \xi^2} - 2\frac{\partial \phi}{\partial \xi}\frac{\partial \phi}{\partial \eta}\frac{\partial^2 \phi}{\partial \xi \partial \eta} + \left(\frac{\partial \phi}{\partial \xi}\right)^2\frac{\partial^2 \phi}{\partial \eta^2}\right]\right. \\ &\cdot\left(\frac{\partial x}{\partial \eta}\frac{\partial f}{\partial \xi} - \frac{\partial x}{\partial \xi}\frac{\partial f}{\partial \eta}\right) + \left[\left(\frac{\partial \phi}{\partial \eta}\right)^2\frac{\partial^2 x}{\partial \xi^2} - 2\frac{\partial \phi}{\partial \xi}\frac{\partial \phi}{\partial \eta}\frac{\partial^2 x}{\partial \xi \partial \eta}\right. \\ &\left.\left. + \left(\frac{\partial \phi}{\partial \xi}\right)^2\frac{\partial^2 x}{\partial \eta^2}\right]\left(\frac{\partial \phi}{\partial \xi}\frac{\partial f}{\partial \eta} - \frac{\partial \phi}{\partial \eta}\frac{\partial f}{\partial \xi}\right)\right\} \end{aligned} \tag{B.4}$$

$$\begin{aligned} \frac{\partial^2 f}{\partial \phi^2} &= \frac{1}{J^2}\left[\left(\frac{\partial x}{\partial \eta}\right)^2\frac{\partial^2 f}{\partial \xi^2} - 2\frac{\partial x}{\partial \xi}\frac{\partial x}{\partial \eta}\frac{\partial^2 f}{\partial \xi \partial \eta} + \left(\frac{\partial x}{\partial \xi}\right)^2\frac{\partial^2 f}{\partial \eta^2}\right] \\ &+ \frac{1}{J^3}\left\{\left[\left(\frac{\partial x}{\partial \eta}\right)^2\frac{\partial^2 \phi}{\partial \xi^2} - 2\frac{\partial x}{\partial \xi}\frac{\partial x}{\partial \eta}\frac{\partial^2 \phi}{\partial \xi \partial \eta} + \left(\frac{\partial x}{\partial \xi}\right)^2\frac{\partial^2 \phi}{\partial \eta^2}\right]\right. \\ &\cdot\left(\frac{\partial x}{\partial \eta}\frac{\partial f}{\partial \xi} - \frac{\partial x}{\partial \xi}\frac{\partial f}{\partial \eta}\right) + \left[\left(\frac{\partial x}{\partial \eta}\right)^2\frac{\partial^2 x}{\partial \xi^2} - 2\frac{\partial x}{\partial \xi}\frac{\partial x}{\partial \eta}\frac{\partial^2 x}{\partial \xi \partial \eta} + \right. \\ &\left.\left. + \left(\frac{\partial x}{\partial \xi}\right)^2\frac{\partial^2 x}{\partial \eta^2}\right]\left(\frac{\partial \phi}{\partial \xi}\frac{\partial f}{\partial \eta} - \frac{\partial \phi}{\partial \eta}\frac{\partial f}{\partial \xi}\right)\right\} \end{aligned} \tag{B.5}$$

$$\frac{\partial}{\partial\phi}\left(r\,\frac{\partial f}{\partial m}\right) = \frac{\partial^2 f}{\partial\phi\partial x} = \frac{1}{J^2}\left[\left(\frac{\partial x}{\partial\xi}\frac{\partial\phi}{\partial\eta} + \frac{\partial x}{\partial\eta}\frac{\partial\phi}{\partial\xi}\right)\frac{\partial^2 f}{\partial\xi\partial\eta} - \frac{\partial x}{\partial\xi}\frac{\partial\phi}{\partial\xi}\frac{\partial^2 f}{\partial\eta^2}\right.$$

$$- \frac{\partial x}{\partial\eta}\frac{\partial\phi}{\partial\eta}\frac{\partial^2 f}{\partial\xi^2}\Big] + \frac{\partial f}{\partial\eta}\left[\frac{1}{J^3}\left(\frac{\partial x}{\partial\xi}\frac{\partial\phi}{\partial\xi}\frac{\partial J}{\partial\eta} - \frac{\partial x}{\partial\eta}\frac{\partial\phi}{\partial\xi}\frac{\partial J}{\partial\xi}\right)\right.$$

$$+ \frac{1}{J^2}\left(\frac{\partial x}{\partial\eta}\frac{\partial^2\phi}{\partial\xi^2} - \frac{\partial x}{\partial\xi}\frac{\partial^2\phi}{\partial\xi\partial\eta}\right)\Big] + \frac{\partial f}{\partial\xi}\left[\frac{1}{J^3}\left(\frac{\partial x}{\partial\eta}\frac{\partial\phi}{\partial\eta}\frac{\partial J}{\partial\xi} - \frac{\partial x}{\partial\xi}\frac{\partial\phi}{\partial\eta}\frac{\partial J}{\partial\eta}\right)\right.$$

$$+ \frac{1}{J^2}\left(\frac{\partial x}{\partial\xi}\frac{\partial^2\phi}{\partial\eta^2} - \frac{\partial x}{\partial\eta}\frac{\partial^2\phi}{\partial\xi\partial\eta}\right)\Big] \qquad \text{(B.6)}$$

Directional Derivatives†

In most fluid flow analyses, the directional derivatives of the flow properties, along or normal to the boundaries, are often needed to evaluate various boundary conditions. These quantities can be easily obtained if the unit vectors tangent or normal to a line of constant ξ or η, that coincide with the physical boundaries, are specified. As pointed out in reference [12], these vectors can be expressed in terms of the transformation parameters $\frac{\partial x}{\partial\xi}$, $\frac{\partial x}{\partial\eta}$, $\frac{\partial\phi}{\partial\xi}$, etc. as follows:

$$(\bar{e}_t)_\xi = -\left(\frac{\partial x}{\partial\eta}\,\bar{e}_m + \frac{\partial\phi}{\partial\eta}\,\bar{e}_\phi\right)/\sqrt{\delta}$$

$$(\bar{e}_t)_\eta = \left(\frac{\partial x}{\partial\xi}\,\bar{e}_m + \frac{\partial\phi}{\partial\xi}\,\bar{e}_\phi\right)/\sqrt{\gamma}$$

† Some of the relations given in this appendix can be found in reference [12]. They are repeated here however for completeness and easy reference for the development of the governing equations.

$$(\bar{e}_n)_\xi = (\frac{\partial \phi}{\partial \eta}\ \bar{e}_m - \frac{\partial x}{\partial \eta}\ e_\phi)/\sqrt{\delta}$$

$$(\bar{e}_n)_\eta = (-\frac{\partial \phi}{\partial \xi}\ \bar{e}_m + \frac{\partial x}{\partial \xi}\ \bar{e}_\phi)/\sqrt{\gamma} \qquad \text{(B.7)}$$

Where $(\bar{e}_t)_\xi$ and $(\bar{e}_t)_\eta$ represent the unit vectors tangent to constant ξ and constant η lines respectively. While, $(\bar{e}_n)_\xi$ and $(\bar{e}_n)_\eta$ denote the unit vectors normal to the constant ξ and the constant η lines. The above mentioned unit vectors are shown in Fig. B-1 as they appear in the physical domain.

The transformation parameters δ and γ in equation (B.7) are given by

$$\delta = (\frac{\partial x}{\partial \eta})^2 + (\frac{\partial \phi}{\partial \eta})^2 \quad , \quad \gamma = (\frac{\partial x}{\partial \xi})^2 + (\frac{\partial \phi}{\partial \xi})^2 \qquad \text{(B.7a)}$$

The directional derivative of any scalar function, f, in any direction $\bar{e}$ is given by

$$\frac{\partial f}{\partial n} = (\bar{e} \cdot \nabla) f$$

where ∇f can be written as

$$\nabla f = \frac{1}{rJ}\ [(\frac{\partial \phi}{\partial \eta}\ \frac{\partial f}{\partial \xi} - \frac{\partial \phi}{\partial \xi}\ \frac{\partial f}{\partial \eta})\ \bar{e}_m + (\frac{\partial x}{\partial \xi}\ \frac{\partial F}{\partial \eta} - \frac{\partial x}{\partial \eta}\ \frac{\partial f}{\partial \xi})\ \bar{e}_\phi] \qquad \text{(B.8)}$$

Associating the direction $\bar{e}$ with the unit vectors normal and tangent to lines of constant ξ or η, we have

$$\frac{\partial f}{\partial (\bar{e}_t)_\xi} = [(\bar{e}_t)_\xi \cdot \nabla] f = -\frac{\partial f}{\partial \eta}/\sqrt{\delta}$$

$$\frac{\partial f}{\partial (\bar{e}_t)_\eta} = [(\bar{e}_t)_\eta \cdot \nabla] f = \frac{\partial f}{\partial \xi}/\sqrt{\gamma}$$

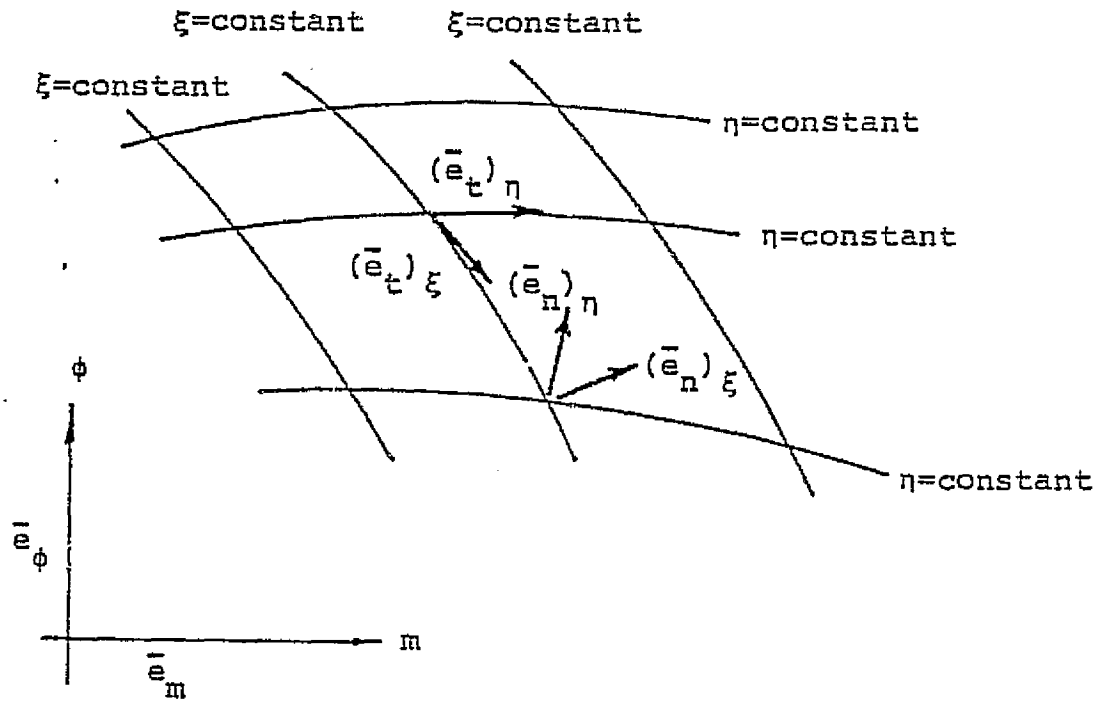

FIG. B-1. UNIT TANGENT AND NORMAL VECTORS.

$$\frac{\partial f}{(\partial \bar{e}_n)_\xi} = [(\bar{e}_n)_\xi \cdot \nabla] f = (\alpha \frac{\partial f}{\partial \xi} - \beta \frac{\partial f}{\partial \eta}) / J\sqrt{\delta}$$

$$\frac{\partial f}{(\partial \bar{e}_n)_r} = [(\bar{e}_n)_\eta \cdot \nabla] f = (\gamma \frac{\partial f}{\partial \eta} - \beta \frac{\partial f}{\partial \xi}) / J\sqrt{\gamma} \qquad \text{(B.9)}$$

where

$$\beta = \frac{\partial x}{\partial \xi} \frac{\partial x}{\partial \eta} + \frac{\partial \phi}{\partial \xi} \frac{\partial \phi}{\partial \eta} \qquad \text{(B.10)}$$

With these relations the different derivative boundary conditions associated with the flow governing equations may be evaluated in a straightforward manner, providing that the values of the different transformation parameters are available.

EN DATE - 10/24-79